PB80-218613

Support Studies in Fluidized-Bed Combustion

Argonne National Lab., IL

Prepared for

Department of Energy
Washington, DC

Aug 80

U.S. Department of Commerce
National Technical Information Service
NTIS.

PB80-218613

Distribution Category:
Coal Conversion and Utilization--
Direct Combustion of Coal
(UC-90e)

EPA-600/7-80-156
August 1980

ANL/CEN/FE-79-14

ARGONNE NATIONAL LABORATORY
9700 South Cass Avenue
Argonne, Illinois 60439

SUPPORT STUDIES IN FLUIDIZED-BED COMBUSTION
Annual Report

October 1978-September 1979

by

Irving Johnson, K. M. Myles, W. M. Swift, S. H. D. Lee,
J. A. Shearer, A. A. Siczek, F. G. Teats, W. I. Wilson, W. A. Boyd,
E. B. Smyk, and C. B. Turner

Chemical Engineering Division

Prepared for the
U. S. Department of Energy
under Contract No. W-31-109-Eng-38
and the
U. S. Environmental Protection Agency
under Agreement IAG-D5-E681

Previous reports in this series

ANL/CEN/FE-78-10	July 1977-September 1978
ANL/CEN/FE-79-3	October-December 1978
ANL/CEN/FE-79-5	January-March 1979
ANL/CEN/FE-79-8	April-June 1979

REPRODUCED BY
NATIONAL TECHNICAL
INFORMATION SERVICE
U.S. DEPARTMENT OF COMMERCE
SPRINGFIELD, VA 22161

TECHNICAL REPORT DATA
(Please read Instructions on the reverse before completing)

1. REPORT NO. EPA-600/7-80-156	2. IERL-RTP-1082
3. RECIPIENT'S ACCESSION NO. PB80 218613	
4. TITLE AND SUBTITLE Support Studies in Fluidized-bed Combustion, Annual Report, October 1978-September 1979	5. REPORT DATE August 1980 Issuing Date.
	6. PERFORMING ORGANIZATION CODE
7. AUTHOR(S) I. Johnson, K. M. Myles, W. Swift, S. Lee, J. Shearer, A. Siczek, F. G. Teats, W. I. Wilson, W. Boyd, E. Smyk, and C. Turner	8. PERFORMING ORGANIZATION REPORT NO. ANL/CEN/FE-79-14
9. PERFORMING ORGANIZATION NAME AND ADDRESS Argonne National Laboratory 9700 South Cass Avenue Argonne, Illinois 60439	10. PROGRAM ELEMENT NO. EHE623A
	11. CONTRACT/GRANT NO. EPA-IAG-D5-E681 DoE-W31-109-ENG-38
12. SPONSORING AGENCY NAME AND ADDRESS EPA, Office of Research and Development* Industrial Environmental Research Laboratory Research Triangle Park, NC 27711	13. TYPE OF REPORT AND PERIOD COVERED Annual; 10/78-9/79
	14. SPONSORING AGENCY CODE EPA/600/13 and DoE

15. SUPPLEMENTARY NOTES IERL-RTP project officer is D. A. Kirchgessner; for details contact IERL=RTP's J. O. Milliken, MD-61, 919/541-4125. (*) Co-sponsored by DoE. EPA-600/7-77-138 and -79-203 are earlier related reports.

16. ABSTRACT The report gives results of working in support of development studies for atmospheric and pressurized fluidized-bed coal combustion. Laboratory and process development studies are aimed at providing needed information on limestone utilization, removal of particulates and alkali metal compounds from the flue gas, control of SO2 and trace pollutant emissions, the mechanism of attrition in fluidized beds, a method of determining the attrition resistance of sorbents, and other aspects of fluidized-bed coal combustion.

17. KEY WORDS AND DOCUMENT ANALYSIS

a. DESCRIPTORS		b. IDENTIFIERS/OPEN ENDED TERMS	c. COSATI Field/Group
Pollution	Calcium Carbonates	Pollution Control	13B
Coal	Dust	Stationary Sources	21D 11G
Combustion	Alkali Metals	Particulate	21B
Fluidizing	Sorbents	Granular Bed Filters	07A, 13H
Fluidized-Bed Processors		Acoustic Dust Conditioning	13I 07B 07D
Sulfur Oxides	Comminution		
Flue Gases	Leaching		

18. DISTRIBUTION STATEMENT Release to Public	19. SECURITY CLASS (This Report) Unclassified	21. NO. OF PAGES 81
	20. SECURITY CLASS (This page) Unclassified	22. PRICE

EPA Form 2220-1 (9-73)

DISCLAIMER

This report has been reviewed by the Environmental Research Laboratory, U.S. Environmental Protection Agency, Athens, Georgia, and approved for publication. Approval does not signify that the contents necessarily reflect the views and policies of the U.S. Environmental Protection Agency, nor does mention of trade names or commercial products constitute endorsement or recomendation for use.

TABLE OF CONTENTS

	Page
ABSTRACT	1
SUMMARY	1
TASK A. HOT GAS CLEANUP	7
1. Removal of Alkali Metal Compounds from Hot Flue Gas	7
a. Effect of NaCl Vapor Concentration in Flue Gas on the Sorption Performance of Diatomaceous Earth and Activated Bauxite	7
b. Ultimate NaCl Vapor Sorption Capacity of Diatomaceous Earth and Activated Bauxite	11
c. NaCl Adsorption and Water-Leaching Regeneration of Activated Bauxite	11
d. Mechanisms of Sorption of NaCl Vapor by Diatomaceous Earth and Activated Bauxite	14
e. Preliminary Economic Evaluations of Diatomaceous Earth and Activated Bauxite Used for the Removal of Alkali Metal Compounds from Hot Flue Gas of PFBC	15
f. Future Work	16
2. Particle Removal from Flue Gas	16
a. Acoustic Dust Conditioning	17
b. High-Efficiency Cyclone	20
TASK B. TRACE POLLUTANTS IN THE FLUIDIZED-BED COMBUSTION OF COAL	46
TASK C. LIMESTONE UTILIZATION	48
1. Enhancement of Limestone Utilization by Hydration	48
a. Laboratory Studies	48
2. Development of Process Flow Sheet for Spent Sorbent Hydration	57
3. Limestone Attrition Characterization	62
a. Effect of Calcination	62
b. Test During Attrition Experiments	63
4. Studies of Sulfation Process in FBC	68
REFERENCES	72

LIST OF FIGURES

No.	Title	Page
1.	Average Rate of NaCl Sorption of Activated Bauxite as a Function of NaCl Vapor Concentration in Flue Gas	10
2.	Effect of NaCl Vapor Concentration in Flue Gas on NaCl Capture of Activated Bauxite as a Function of Experimental Duration	10
3.	NaCl Vapor Sorption Capacity of Diatomaceous Earth and Activated Bauxite as a Function of Experiment Duration at 800°C and Atmospheric Pressure	12
4.	NaCl Vapor Sorption by Water-Leached Regenerated Activated Bauxite as a Function of Sorption and Regeneration Cycle	14
5.	Schematic of the Pulse Jet/Resonant Maniford System	17
6.	Schematic Flowsheet of the Pressurized Fluidized-Bed Combustion System	21
7.	TAN-JET Tube	22
8.	Dimensional Schematic of the TAN-JET Cyclone	23
9.	Penetration of Flue Gas Particulate Matter Through TAN-JET Cyclone as a Function of Mass Loading in Flue Gas Entering the Cyclone	26
10.	Penetration and Particle Loading in Flue Gas Leaving TAN-JET Cyclone as a Function of Particle Loading Entering TAN-JET Cyclone for Secondary Air Nozzle. $\Delta P \cong 70$ kPa	29
11.	Penetration and Particle Loading in Flue Gas Leaving TAN-JET Cyclone as a Function of Particle Loading Entering TAN-JET Cyclone for Secondary Air Nozzle. $\Delta P \cong 105$ kPa	30
12.	Penetration and Particle Loading in Flue Gas Leaving TAN-JET Cyclone as a Function of Particle Loading Entering TAN-JET Cyclone for Secondary Air Nozzle. $\Delta P \cong 140$ kPa	31
13.	Particle Loadings in Flue Gas Leaving the PDU Combustor during Operation at 810 kPa and 875°C	34
14.	Primary Cyclone Performance Related to Solids Loading in Flue Gas Entering the Cyclone	34

LIST OF FIGURES (contd)

No.	Title	Page
15.	Primary Cyclone Performance Related to Gas Flow Through the Cyclone	35
16.	TAN-JET Cyclone Performance Related to Solids Loading in Flue Gas Entering the Cyclone	36
17.	TAN-JET Cyclone Performance Related to Gas Flow Through the Cyclone	37
18.	TAN-JET Performance Characteristics as Function of Secondary Air Nozzle Pressure Drop with TAN-JET as Primary Cyclone	38
19.	Particle Size Distributions of Fly Ash Recovered from TAN-JET Cyclone Hopper	41
20.	Particle Size Distributions for Samples of Fly Ash Filtered from Flue Gas Downstream from TAN-JET Cyclone	41
21.	Comparison of Concentrations of Particles in Flue Gas Leaving TAN-JET Cyclone as a Function of Particle Diameter, Along with Estimates of Acceptable Distributions for Gas Turbines	43
22.	Calculated Particle Size Distributions of Dust Entering TAN-JET Cyclone	44
23.	Calculated Grade Efficiency Curves for TAN-JET Cyclone	45
24.	Porosimetry Curves for ANL-9501 Showing the Effect of Water Treatment and Subsequent Resulfation on Partially Sulfated Fluidized-Bed Combustor ANL-9501 Samples	49
25.	Porosimetry Curves for Spent ANL-9501 Limestone Sprayed with Water and Resulfated at 850°C in a Laboratory-Scale Fluidized Bed	50
26.	Pore Distribution for Sulfated and Water-Treated ANL-9501 Sorbent Prior to Resulfation	54
27.	Pore Distribution for Hydrated "Spent" ANL-9501 Sorbent after Calcination for 1 h at 850°C in 5% O_2, 20% CO_2, and the Balance N_2	55
28.	Pore Distributions for Steady-State Overflow Samples of ANL-9501 Sorbent from Combustor at 850°C after Successive Cycles of Sulfation-Hydration	55

LIST OF FIGURES (contd)

No.	Title	Page
29.	Low-Temperature DTA Curves for FBC Overflow Material	57
30.	High-Temperature DTA Curves for FBC Overflow Material	58
31.	Limestone ANL-9501 Partially Sulfated and Hydrated in a Laboratory Fluidized Bed	59
32.	Two Views of a Particle of Limestone ANL-9501 After Partially Sulfated, Treated with Water, and Fed to a Fluidized-Bed Coal Combustor at 850°C	60
33.	Cooler-Hydrator for Water Treatment of Sulfated Sorbent	61
34.	Laboratory-Scale Fluidized-Bed Apparatus for Attrition Experiments	65
35.	Particle Size Distribution of ANL-5101. Initial particle diameter, 1410-1190 μm	67
36.	Particle Size Distribution of ANL-5101. Initial particle diameter, 1000-841 μm	68
37.	Sulfated ANL-9501 Particles Produced at Different Bed Temperatures in the Atmospheric Fluidized-Bed Coal Combustor	69
38.	Interior View of ANL-9501 Particle, Sulfated in Fluidized-Bed Coal Combustor at 800°C, Showing Uncalcined Limestone	70
39.	Porosimetry Curves for Fluidized-Bed Coal Combustor Samples of ANL-9501 Limestone Sulfated at Different Bed Temperatures	71

LIST OF TABLES

No.	Title	Page
1.	Distributions of NaCl from Testing Activated Bauxite for NaCl Vapor Capture as a Function of Experiment Duration and NaCl Vapor Concentration in the Flue Gas	9
2.	Evaluation of Cost of Granular Sorbents for 97% Alkali Removal and 80% Sulfur Removal for a 200-MWe PFBC Demonstration Plant	16
3.	Design Configuration of TAN-JET Cyclone and Other Cyclone Designs	24
4.	TAN-JET Cyclone Experiments at Ambient Temperature	25
5.	Elevated-Temperature TAN-JET Cyclone Experiments (System pressure: ≈305 kPa absolute)	28
6.	Elevated-Temperature TAN-JET Cyclone Experiments (System pressure: ≈810 kPa absolute)	33
7.	Conditions and Results of Experiments with TAN-JET as the Primary Cyclone	39
8.	Particle Loading Downstream from TAN-JET by Particle Size Range	42
9.	Laboratory Quartz Fluidized-Bed Hydration at 100°C of Partially Sulfated Limestone	51
10.	Enhancement of Sulfur Retention of Various Limestones and Dolomites by Hydration Treatment	52
11.	Chemical Composition of Limestone	63
12.	Effect of Calcination, Sulfation, and Estimated Attrition Resistance in Fluidized Beds on Limestone Particles	64
13.	Effect on Limestone Particle Size of Attrition in a Fluidized Bed at 900°C	66
14.	Operating Conditions for 6-in.-dia Fluidized-Bed Coal Combustor with Various Sorbent Feeds	71

SUPPORT STUDIES IN FLUIDIZED-BED COMBUSTION
ANNUAL REPORT

October 1978-September 1979

by

Irving Johnson, K. M. Myles, W. M. Swift, S. H. D. Lee,
J. A. Shearer, A. A. Siczek, F. G. Teats, W. I. Wilson, W. A. Boyd,
E. B. Smyk, and C. B. Turner

ABSTRACT

This work supports the development studies for atmospheric and pressurized fluidized-bed coal combustion. Laboratory and process development studies are aimed at providing needed information on limestone utilization, removal of particulates and alkali metal compounds from the flue gas, control of SO_2 and trace pollutant emissions, the mechanism of attrition in fluidized-beds, a method of determining the attrition resistance of sorbents, and other aspects of fluidized-bed coal combustion.

SUMMARY

Task A. Hot Gas Cleanup

Removal of Alkali Metal Compounds from Hot Flue Gas

The use of diatomaceous earth and activated bauxite as solid granular sorbents for the removal of gaseous alkali metal compounds (viz., NaCl, KCl, or K_2SO_4) from the hot combustion gas of coal continues to be studied. In these studies, a hot (800°C) simulated flue gas of PFBC loaded with a gaseous alkali metal compound passes through a hot packed bed of the granular sorbent being tested to determine the effectiveness of the sorbent for removing the alkali vapors.

Experimental tests have been made (1) to determine the effect of NaCl vapor concentration in the flue gas on the sorption performance and ultimate alkali sorption capacities of diatomaceous earth and activated bauxite and (2) to investigate the regenerability of activated bauxite by water-leaching. The average rate of NaCl vapor sorption for both sorbents was found to be a linear function of NaCl vapor concentration in the flue gas. Reduction in NaCl vapor concentration did not reduce the sorption efficiencies of either sorbent. The ultimate sorption capacity of activated bauxite was found to be about 25 mg NaCl/g sorbent, while the ultimate sorption capacity of diatomaceous earth was much greater but was not measured in the tests conducted.

Experimental evidence indicates that the sorption of NaCl vapor by diatomaceous earth is due to the chemical reaction of diatomaceous earth with NaCl vapor to form water-insoluble sodium silicates. In contrast, activated bauxite captures NaCl vapor mainly through an adsorption mechanism. Since an adsorption process is a reversible process, activated bauxite is regenerable. Tests have demonstrated that activated bauxite can be easily regenerated by a simple water-leaching process and that the regenerated activated bauxite maintains a sorption activity similar to that of fresh activated bauxite.

Cost evaluations have been made as preliminary estimates of the costs of diatomaceous earth and activated bauxite used as granular sorbents for the removal of alkali vapors from the hot flue gas of PFBC's. Results indicate that on a once-through basis, the cost of activated bauxite is about twice that of diatomaceous earth; however, the cost of activated bauxite can be significantly reduced if calculated on the basis of regeneration.

Particle Removal from Flue Gas

In PFBC, the hot flue gas from the combustor must be expanded through a gas turbine to recover energy and make the process economic. To prevent unacceptable erosion of the turbine blades by particles of limestone and fly ash present in the flue gas, the particle loading must be reduced to low, but not well-defined, levels. There is considerable concern that existing particulate control technology may be inadequate at the high-temperature, high-pressure environment of the PFBC flue gas. This report presents (1) a summary of the progress which was made in developing a pulse-jet resonant manifold system for investigating acoustic dust conditioning as a pre-conditioning step in particulate removal and (2) the results of testing a high-efficiency cyclone.

Acoustic Dust Conditioning. Work was continued at the University of Toronto, under subcontract to ANL, to develop a pulse-jet acoustic dust-conditioning system for subsequent testing and evaluation at ANL. Acoustic dust conditioning is defined as the process whereby the natural tendency of particles to agglomerate is enhanced by exposure of the particles to high-intensity acoustic fields. The effort at the University of Toronto was scheduled to be completed in three phases. Phase I was completed; it consisted of the design, fabrication, and testing of a pulse-jet resonant manifold system (PJ-RMS) at atmospheric pressure. Sound intensities were as high as 160 dB at frequencies of 300 to 350 Hz.

Phase II, increasing the operating pressure of the PJ-RMS to about 1.01 MPa, was in progress when the project was discontinued due to budgetary factors. During Phase II, the operating pressure of the pulse-jet had been increased to 350 kPa, with indications that the increase in pressure had increased the sound levels obtainable.

Phase III, which was to be the design, manufacture, and testing of pulse-jet acoustical agglomeration in the ANL fluidized-bed combustion flue gas system, was not completed.

The results of work completed at the University of Toronto yield no evidence that the technical objectives of the project were unobtainable. However, the project did require significantly more developmental work than was originally anticipated. Continued examination of acoustic dust conditioning for high-temperature/high-pressure applications is recommended.

TAN-JET Cyclone. A Donaldson Co. TAN-JET cyclone, claimed to have a particle removal efficiency superior to that of conventional cyclones, was installed in the ANL fluidized-bed combustor flue gas system for testing and evaluation. The TAN-JET employs a secondary flow of "clean" air through a nozzle located inside the cyclone. The Donaldson design provides for the secondary air entering the cyclone at sonic velocity.

A large number of tests have been performed with the TAN-JET cyclone to measure its particle-removal efficiency. Experiments have been performed (1) at low pressure, either at about 240 kPa with fluidization of limestone in the combustor but no coal combustion or at 305 kPa in combustion experiments, and (2) at high pressure (810 kPa) in combustion experiments.

In the lower-pressure experiments (240 and 305 kPa), loadings in the flue gas entering the TAN-JET were between about 0.5 and 3.5 g/m^3. These loadings were typical of those in gas from a primary cyclone stage of gas cleaning. At pressure drops across the secondary air nozzle of either about 105 and 140 kPa (less than that required for sonic velocity), the loadings in the flue gas leaving the TAN-JET were as low as 0.08 g/m^3 and no higher than 0.17 g/m^3. The combined particle-removal efficiency of the primary and TAN-JET cyclones in series was about 99.5% in the low-pressure combustion experiments.

In the high-pressure (810-kPa) experiments, loadings in the flue gas entering the TAN-JET ranged from about 1.0 to 6.0 g/m^3. In certain of these experiments, the primary cyclone was apparently overloaded, resulting in high inlet loadings to the TAN-JET. At these conditions, loadings in the flue gas leaving the TAN-JET were between 0.1 and 0.2 g/m^3 at the higher (105 and 140 kPa) secondary air nozzle pressure drops.

A few tests were also performed with the primary cyclone removed from the system. Loadings to the TAN-JET during these experiments were between 20 and 29 g/m^3. The TAN-JET cyclone generally exhibited a particle-removal efficiency of 99% or better at a nozzle pressure drop of 140 kPa.

Selected samples from two combustion experiments (one at 305 kPa and one at 810 kPa) were obtained for particle size analyses of the stone. The information obtained was used to determine grade efficiency curves for the TAN-JET at conditions (except pressure) that were nominally similar. Indicated 50% cut points for the TAN-JET cyclone are about 0.9 μm for the low-pressure experimental data, about 1.6 μm for the high-pressure experimental data. A vendor-supplied performance curve indicated a somewhat higher 50% cut point--about 2.0 μm.

Comparison of the loadings and size distributions of the dust passing through the TAN-JET for the above two experiments with loadings and size distributions suggested to be acceptable for gas turbines gave mixed results.

In the case of the data from the 810-kPa experiment, the cumulative loading distribution by particle size generally exceeded that estimated to be acceptable. The results for the 305-kPa experiment indicated, however, that for particles larger than about 3 μm, the experimental cumulative loading by particle size fell within the range of conditions estimated to be acceptable.

Task B. Trace Pollutants in the Fluidized-Bed Combustion of Coal

The objective of this task is to develop methods of reducing the environmental impact of fluidized-bed combustion. The health and ecological effects of organic compounds and inorganic trace elements released from the FBC system will be addressed. The studies will include the identification of organic and inorganic constituents in the effluent streams (fly ash and stack gases) and evaluation of radioactivity associated with coal combustion; identification of the FBC conditions and factors affecting combustion efficiencies and pollution; and identification of methods of removing the pollutants (e.g., further catalytic burnup, condensation/adsorption, and adsorption/desorption of vapors).

Task C. Limestone Utilization

Enhancement of Limestone Sulfation by Hydration. Laboratory Studies. The in situ formation of $Ca(OH)_2$ in partially sulfated "spent" limestone has been found to enhance further sulfation of the stone when the stone is reintroduced into a coal combustor. The changes in pore distribution upon dehydration (seen in combustor samples of once-hydrated ANL-9501 limestone) account for the increase in sulfation and sulfation capacity of partially spent limestones.

Laboratory experiments on fluidized-bed hydration of "spent" material have proved successful with several limestones; hydration was accomplished at low temperatures by direct spraying of water or by the introduction of steam.

Total sulfation of a variety of limestones (9) and dolomites (6) has increased dramatically after hydration. Visual inspection of the material provides a rough estimate of the extent of decrepitation induced by the expansion due to hydration.

Several general conclusions can be drawn on the basis of the results of laboratory studies, which have also been supported by examination of PDU-scale experimental samples. Increases were found in total porosity, average pore diameter, initial surface area, and particle size due to particle expansion offset by increased decrepitation. After treatment with water, total sulfation was greater in all cases.

The grain size within particles decreases as CaO is recrystallized from $Ca(OH)_2$ during dehydration. In general, upon water treatment, dolomites exhibit little or no decrepitation and there is a much smaller physical effect than for limestones. Decrepitation in limestones depends on several variables, including original porosity, the concentrations of impurities including MgO, percent $CaSO_4$, and the technique and temperature of water treatment. Precalcination following hydration increases the extent and rate of sulfation.

Several cyclic experiments have been performed on a process development unit (PDU) atmospheric fluidized-bed coal combustor. Pore distributions of the various materials from each cycle were characterized; changes in total porosity and gradual increases in average pore diameter were observed.

Differential thermal analysis (DTA) measurements were also made on these cycled samples to determine the distribution of water within the particle. Results show that almost 100% of the adsorbed water is in the form of $Ca(OH)_2$ rather than hydrated calcium sulfate.

Scanning electron microphotographs (SEMs) of laboratory and combustor samples that had been treated with water and calcined or resulfated show increased pore size and total porosity, expanded macrostructure, and decreased crystallite size of the material.

Development of Process Flowsheet for Spent Sorbent Hydration. A scheme is presented to increase the reactivity with SO_2 of partially sulfated sorbent from fluidized-bed combustion by hydrating it with water in large-scale systems.

Limestone Attrition Characterization. Natural sorbents are being tested in a laboratory-scale fluidized bed for their attrition resistance as a function of their physical and chemical properties (for example, the extent of calcination or sulfation, and the predominant grain size). The objectives of this study are (1) to determine the mechanism of attrition in fluidized beds and (2) to develop a relatively simple method of determining the attrition resistance of sorbents in fluidized-bed coal combustors.

The effect of calcination on particle size was determined for several limestones. In contrast to other stones previously tested under similar conditions, they did not break up when calcined (i.e., the stones were not "poppers"). However, when some of the stones were tested for probable resistance to attrition under fluidized-bed conditions, calcination seemed to have softened the stones, causing them to lose their integrity.

In a series of experiments, Tymochtee dolomite (ANL-5101 limestone) was tested to determine the effect of attrition on the distribution of particle size in a laboratory-scale fluidized-bed (quartz vessel) combustor. Fluidized-bed attrition tests were done on two particle size ranges, 1410–1190 μm (-14 +16 mesh) and 1000–841 μm (-18 +20 mesh), for 15, 30, and 120 min. For the material of 1410–1190 μm particle diameter, approximately 63 wt % of the particles retained their original diameters at the end of the tests. For the particle size range, 1000–841 m, approximately 85 wt % of the particles had the same particle diameters at the end of the tests as the original starting material. Comparison of the results for the two particle size ranges seems to show that there is a greater shift in particle diameter for the 1410–1190 m material than for the 1000–841 m material. However, for material of both size ranges, results suggest that after 15 min, the attrition rate is constant (at zero) in all test runs.

Studies of Sulfation Process in FBC. Scanning electron microphotographs have been made of limestone particles sulfated at three temperatures (800, 850, and 900°C) in the atmospheric fluidized-bed coal combustor.

At 800°C, an increased pore diameter at higher temperatures was observed, as well as incomplete calcination of the material. Characterization of combustor samples is necessary to allow their comparison with laboratory samples and ultimately an understanding of differences in reactivity of the two.

TASK A. HOT GAS CLEANUP

1. Removal of Alkali Metal Compounds from Hot Flue Gas

(S. H. D. Lee, W. A. Boyd, and W. M. Swift)

In the prospective application of pressurized fluidized-bed combustion (PFBC) of coal for power generation, the corrosion of turbine blades (of gas turbines in combined-cycle power plants) due to attack by alkali metal compounds present in the hot flue gas appears to be a potential problem. This problem can be eliminated by reducing the concentration of alkali metal compounds in hot flue gas to a level tolerable by a turbine blade. A way to accomplish this is to use granular sorbent in a hot fixed-bed filter to remove the alkali metal compounds from the hot flue gas before it is expanded into a turbine. The objective of this task is to develop an effective sorbent for hot fixed-bed filters.

Previous experiments have shown that activated bauxite and diatomaceous earth are the two most effective sorbents among six commercial products screened. They are very effective in capturing all NaCl, KCl, and K_2SO_4 vapors from a simulated hot PFBC flue gas, indicating the potential of these two sorbents for use as filter media in a granular fixed-bed filter. Experimental results for the screening tests and for the studies on the effects of sorbent bed temperature, superficial gas velocity, and gas hourly space velocity of flue gas on salt retention were presented in the previous annual report (ANL/CEN/FE-78-10).

This study was carried out using a laboratory-scale, batch, fixed-bed combustor system consisting of a preheating section which is preheated at startup, a combustion section where the pure alkali metal compound sample is heated and vaporized, a filtration section containing a packed bed of the sorbent to be tested, and a cold-trap section containing water-cooled metal cold traps. This combustor system was described in detail in an earlier annual report in this series (ANL/ES-CEN-1016).

During this report period, studies have been continued in order to obtain the technical data base needed for the design of granular filters to remove gaseous alkali metal compounds from hot flue gas, with either diatomaceous earth or activated bauxite used as a sorbent. Presented here are experimental results obtained from studies designed (1) to investigate the effect of NaCl vapor concentration in flue gas on the sorption performance of diatomaceous earth and activated bauxite, (2) to obtain the ultimate NaCl-vapor sorption capacities of diatomaceous earth and activated bauxite, (3) to gain a better understanding of the sorption mechanisms of these two sorbents toward NaCl vapor, and (4) to examine the regenerability of activated bauxite by a water-leaching process. Also presented is a preliminary economic evaluation of both sorbents used as filter media in a granular fixed-bed filter for the removal of alkali metal compounds from hot flue gas of PFBC.

a. Effect of NaCl Vapor Concentration in Flue Gas on the Sorption Performance of (1) Diatomaceous Earth and (2) Activated Bauxite

Except in screening tests with K_2SO_4 vapor, tests so far completed were generally conducted using a simulated flue gas of PFBC containing about 80 ppm of alkali metal compound vapor. On the basis of experimental

measurements[1-3] and thermodynamic estimations,[4,5] the alkali vapor concentration in the flue gas of PFBC approaches the order of 10 ppm, depending on operating conditions. Based on this information, studies of the sorption performance of both diatomaceous earth and activated bauxite in flue gas containing low concentrations of alkali metal compound vapors are needed. Therefore, a series of experiments were carried out to test the sorbents in flue gas containing 24 to 107 ppm NaCl vapor. The reason for using an alkali concentration higher than 10 ppm was to obtain a detectable amount of alkali vapor within a reasonable experimental period.

In this series of experiments, sorbents were tested at 800°C and atmospheric pressure, using a simulated dry flue gas of PFBC. The flue gas had a volumetric composition of 3% O_2, 16% CO_2, about 300 ppm SO_2, about 180 ppm H_2O, various amounts of NaCl vapor, and the balance N_2. The superficial gas velocity of flue gas passing through the sorbent bed was 66 cm/s, and the particle size of the sorbent tested was -8 +10 mesh.

The experimentally measured distributions of NaCl obtained from testing diatomaceous earth for NaCl vapor capture as a function of experiment duration and NaCl vapor concentration in the flue gas were reported and discussed in earlier quarterly reports during the past year (ANL/CEN/FE-79-3 and -79-5). It was found that the average rate of NaCl sorption by diatomaceous earth was a linear function of NaCl vapor concentration. The sorption efficiency for diatomaceous earth for removal of NaCl vapor from flue gas was not reduced when NaCl concentration in flue gas was decreased. The sorption efficiency remained at a higher level for longer periods of time at low NaCl concentration than at high NaCl concentration.

Table 1 shows the experimentally measured distributions of NaCl obtained from testing activated bauxite for NaCl vapor capture as a function of experiment duration and NaCl vapor concentration in the flue gas. The results are also plotted in Fig. 1 and 2. Figure 1 is a plot of the average rate of NaCl vapor sorption by activated bauxite in milligrams of NaCl per hour per gram of sorbent as a function of NaCl vapor concentration in parts per million. In Fig. 2, the percent of NaCl vapor captured is plotted as a function of experiment duration in hours.

As shown in Fig. 1, the average rate of NaCl vapor sorption by activated bauxite is a linear function of the NaCl vapor concentration in the flue gas. This linear relationship was observed for both of the gas hourly space velocity conditions tested (GHSVs of 18,600 and 33,500 h^{-1}) and was observed to hold only for a limited duration - longer for lower NaCl vapor concentrations. This phenomenon was also observed for diatomaceous earth.

Of practical importance in the development of a sorbent is the effectiveness of the sorbent in removing alkali metal compounds from flue gas. The effects on the sorption efficiency of activated bauxite of (1) NaCl concentration in the flue gas and (2) experimental duration are shown in Fig. 2. As expected, the efficiency (in terms of percent of the NaCl vapor captured by the activated bauxite) decreases with experimental duration. Figure 2 shows that the same levels of sorption efficiency obtained at the high NaCl vapor concentration (107 ppm) can also be obtained when the NaCl vapor concentration in the flue gas is reduced to about one-third that high value

Table 1. Distributions of NaCl from Testing Activated Bauxite for NaCl Vapor Capture as a Function of Experiment Duration and NaCl Vapor Concentration in the Flue Gas

The sorbent was tested at 800°C and atmospheric pressure in a simulated dry flue gas of PFBC at a linear velocity of 66 cm/s.

	HGC-50	HGC-60	HGC-59	HGC-54	HGC-53	HGC-51	HGC-71	HGC-77	HGC-78	HGC-79
Experiment Duration, h	2	2	3	5	10	2	5	7	10	15
Avg. NaCl Vapor Conc. in Flue Gas, ppm	107	33	35	53	43	107	37	31	32	36
Amount of Sorbent, g	60	27	27	27	27	115	50	50	50	50
GHSV, h^{-1}	←		33,500		→	←		18,600		→
(1) NaCl Collected by Cold Trap and Glass-Wool Filter, mg	30	6	6	23	123	5	3	7	6	49
(2) NaCl Captured by Sorbent,[a] mg	348	44	72	176	201	372	136	157	236	353
(3) Sum [(1) + (2)], mg NaCl	378	50	78	199	324	377	139	164	242	402
(4) Avg. Rate of Sorption, mg NaCl/h-g sorbent	2.90	0.82	0.89	1.30	0.74	1.62	0.54	0.45	0.47	0.47
(5) NaCl Capture, %	92.1	88.0	92.3	88.4	62.0	98.7	97.8	95.7	97.5	87.8

[a] Na concentration of the sorbent was obtained by fusing representative samples of the sorbent with NH_4HF_2, dissolving the samples in distilled water, and then analyzing the solutions using flame emission spectrometry (FE). FE analysis was done by R. Bane.

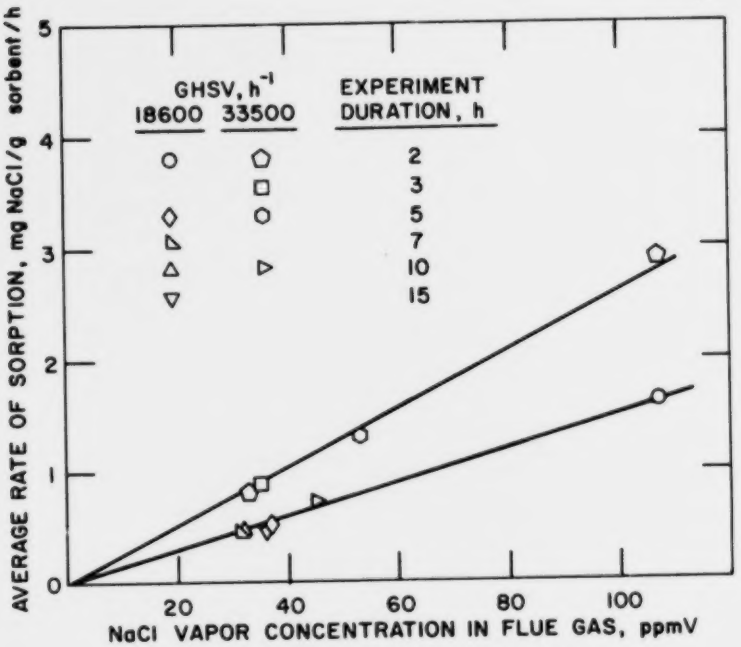

Fig. 1. Average Rate of NaCl Sorption of Activated Bauxite as a Function of NaCl Vapor Concentration in Flue Gas

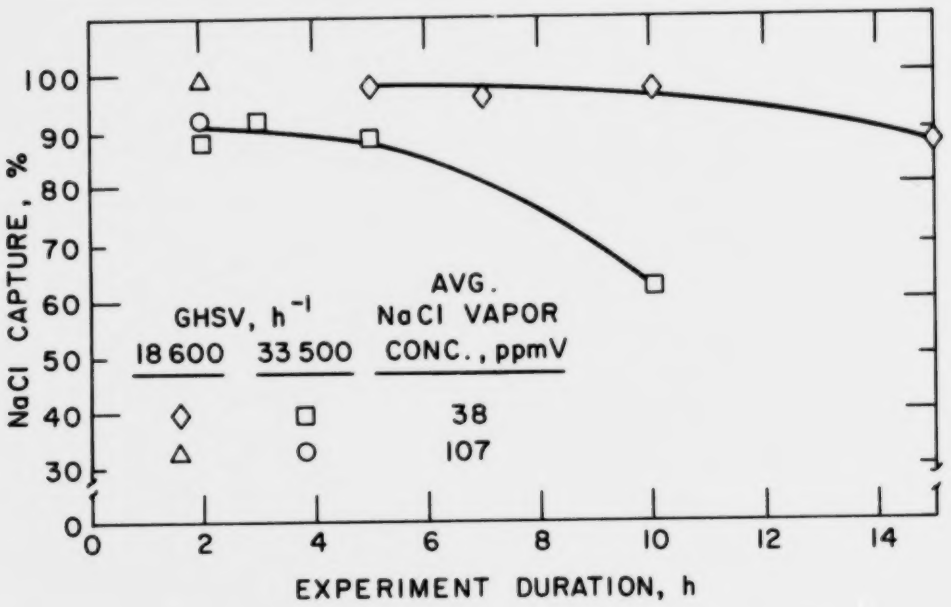

Fig. 2. Effect of NaCl Vapor Concentration in Flue Gas on NaCl Capture of Activated Bauxite as a Function of Experiment Duration

(38 ppm). Figure 2 also shows that at a GHSV of 33,500 h^{-1} (contact time of about 0.1 s), the maximum efficiency achievable is 90%. This maximum efficiency can be increased, however, to greater than 97% by decreasing the GHSV to 18,600 h^{-1}, or by increasing the contact time of the flue gas with the sorbent to about 0.2 s. Similar results were observed for diatomaceous earth sorbent (ANL/CEN/FE-79-3 and -79-5).

It can be concluded from this series of experiments that the average rate of NaCl vapor sorption of activated bauxite is a function of NaCl vapor concentration in flue gas. The reduction of NaCl vapor concentration in flue gas does not reduce the sorption efficiency of activated bauxite.

b. Ultimate NaCl Vapor Sorption Capacity of Diatomaceous Earth and Activated Bauxite

Ultimate sorption capacity is defined as the maximum amount of alkali vapor the sorbent can hold at a given temperature and pressure. A series of tests have been carried out to obtain the ultimate NaCl vapor sorption capacities for diatomaceous earth and activated bauxite. Tests were conducted using the small-scale sorption test rig that has been shown and described in detail in an earlier report in this series (ANL/CEN/FE-78-4).

In this series of tests, only one sorbent particulate layer was used, evenly spread out on platinum gauze, so that each sorbent particle had a maximum and equal chance of being exposed to NaCl-bearing simulated dry flue gas of PFBC. The volumetric composition of the simulated dry flue gas was 3% O_2, 16% CO_2, about 300 ppm SO_2, about 120 ppm H_2O, and the balance N_2.

Figure 3 shows sorption capacities, in mg NaCl per gram of sorbent, plotted as a function of experiment duration in hours, when -8 +10 mesh sorbent was tested at 800°C and atmospheric pressure for two different average NaCl vapor concentrations in flue gas. The superficial gas velocity of flue gas passing through the sorbent layer was 27 cm/s. Under this experimental condition, the sorption of NaCl vapor by both diatomaceous earth and activated bauxite has been shown to be not mass-transfer controlled.[6]

As shown in Fig. 3, the NaCl vapor sorption capacity of activated bauxite initially increases with experiment duration; however, it levels off and approaches to an ultimate sorption capacity of about 25 mg/g sorbent. In contrast, the sorption capacity of diatomaceous earth shows a continuous linear increase to 150 mg NaCl/g sorbent and does not show a leveling-off; therefore, the ultimate NaCl-vapor sorption capacity of diatomaceous earth is much greater than that of activated bauxite, but was not determined in this set of experiments.

c. NaCl Adsorption and Water-Leaching Regeneration of Activated Bauxite

Activated bauxite is not only effective for capturing alkali metal compound vapors (such as NaCl, KCl, and K_2SO_4), but also has a potential for further development in that it can easily be regenerated by a simple water-leaching regeneration process. Its regenerability has been experimentally demonstrated in three cycles of NaCl sorption and water-leaching regeneration

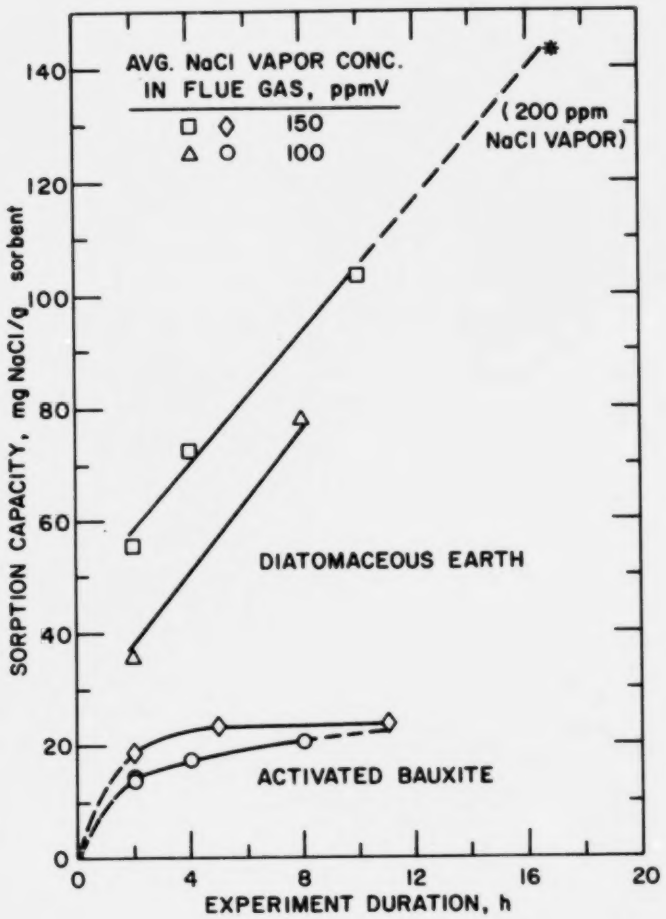

Fig. 3. NaCl Vapor Sorption Capacity of Diatomaceous Earth and Activated Bauxite as a Function of Experiment Duration at 800°C and Atmospheric Pressure

experiments. The sorption performance as a function of sorption-regeneration cycle has also been determined in 10-cycle tests of NaCl sorption and water-leaching regeneration. Results of these two cyclic tests have been presented and discussed in previous quarterly reports (ANL/CEN/FE-79-3 and -79-5).

During the cyclic tests, it was observed that activated bauxite, originally light pink, became milky white after adsorbing NaCl vapor and then was restored to its original light-pink color upon being leached with water. This color-change phenomenon indicates that NaCl vapor, which is milky white in color when condensed, had been adsorbed on the surface of activated bauxite during the adsorption stage and that NaCl had been released from the surface during the water-leaching regeneration stage. The latter is confirmed by analytical results which showed a unity mole ratio of Na^+ to Cl^- in the

leachates. The regenerated activated bauxite was found to gain fair amounts of pore volume in the very fine pores (<0.10 μm). Pore volume increased in later regeneration cycles.

During experimental handling and water-leaching regeneration, some activated bauxite fines were produced due to attrition of the sample. Attrition was greatest in the first cycle--6.6 and 4.0% for 3-cycle and 10-cycle tests, respectively, but dropped afterwards. The average attrition in the 10-cycle test was 2% per cycle.

In the 3-cycle test, the NaCl material balances show that in the first cycle, 24.2 mg NaCl was captured per gram of activated bauxite. This amount cosely approaches the ultimate sorption capacity of activated bauxite at the same experimental sorption conditions (about 25 mg NaCl/g sorbent, as shown in Section 1-b above). Of the amount of NaCl vapor captured, about 51% was water-leachable, indicating that this was the amount of NaCl captured by an adsorption process. The remainder (about 49%) was retained in the activated bauxite. The chemical reactions between the SiO_2 and the clay minerals present as impurities in activated bauxite are believed responsible for retention of that about 49% of the NaCl. In the second and third cycles, the sorption capacities of the regenerated activated bauxite decreased with regeneration cycle, being 22.2 and 16.6 mg NaCl/g sorbent, respectively. This decrease in sorption capacity was due to the loss of chemical reactivity of SiO_2 and clay minerals in activated bauxite. However, the amount of NaCl vapor captured by an adsorption process was noted to increase in the second and third cycles. This indicates that NaCl vapor capture from regenerated activated bauxite is essentially an adsorption process.

An adsorption process is a reversible process--the adsorbent can be used repeatedly to adsorb after each desorption of adsorbate. For a given adsorbate and unit weight of a given adsorbent, the amount of adsorbate sorbed at equilibrium is a function of the final pressure and temperature only;[7] therefore, after about the third cycle, at constant pressure and temperature, the amount of NaCl vapor adsorbed (or the sorption capacity) by activated bauxite by a pure adsorption process should be constant, i.e., independent of adsorption and regeneration cycle. Based on these arguments, the sorption capacity can be maintained at about 16 mg NaCl per g activated bauxite after the third cycle of the adsorption and regeneration process. This sorption capacity was found to be very adequate for greater than 95% removal of NaCl vapor from flue gas by regenerated activated bauxite. Results of the 10-cycle test described below support this finding.

In the 10-cycle tests, activated bauxite was firstly tested for its NaCl removal efficiency with NaCl-bearing simulated dry flue gas of PFBC. The activated bauxite tested then was leache' with distilled water, filtered with a filter paper, and dried in a muffle furnace, and fines were sieved through 10-mesh screen, completing a cycle. Activated bauxite retained on the screen represented the regenerated activated bauxite. Results of this cyclic test were presented in a previous report (ANL/CEN/FE-79-5). The NaCl vapor removal efficiency as a function of regeneration cycle is summarized in Fig. 4. On the average, a removal efficiency of about 98% was achieved for all ten-cycle tests. The amount of makup of the fresh activated bauxite added

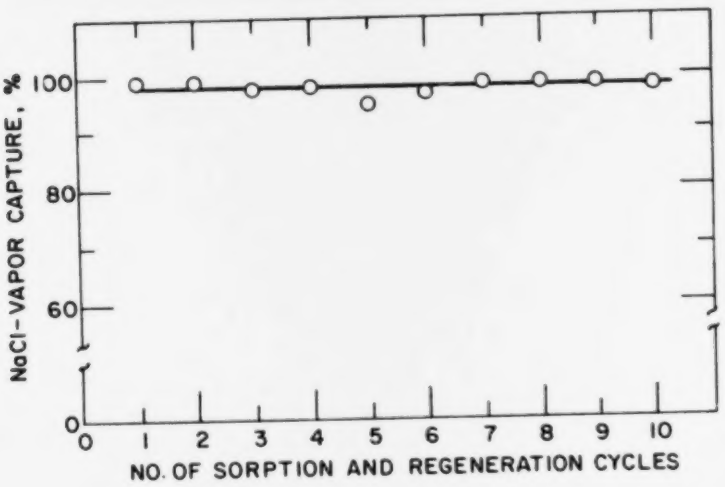

Fig. 4. NaCl Vapor Sorption by Water-Leached Regenerated Activated Bauxite as a Function of Sorption and Regeneration Cycle

to the regenerated activated bauxite constituted only 2% by weight of the total amount of sorbent (50 g); therefore, the consistently very high removal efficiencies observed for the regenerated activated bauxite in the ten cycles indicate that the regenerated activated bauxite is as effective as fresh activated bauxite.

From results of these two cyclic tests, it is concluded that activated bauxite can be effectively regenerated by a simple water-leaching process and that the regenerated activated bauxite behaves as effectively as fresh activated bauxite in capturing NaCl vapor from flue gas.

d. Mechanisms of Sorption of NaCl Vapor by Diatomaceous Earth and Activated Bauxite

Diatomaceous earth is a sedimentary rock of marine or lacustrine deposition. Chemically, it consists primarily of silicon dioxide and various amounts of impurities such as clay, carbonaceous matter, iron oxide, sand, etc. Celatom MP-91 diatomaceous earth, a product of Eagle-Picher Industries, Inc., Ohio, is used in this study. It contains 92% SiO_2, 5% Al_2O_3, and other impurities. Experimental results (Table 5, ANL/CEN/FE-77-11) in a previous report in this series indicated that NaCl vapor captured by diatomaceous earth was primarily in chemical forms that are not soluble in water. The reaction,

$$2\ NaCl(g) + H_2O(g) + n\ SiO_2(s) = Na_2O{\cdot}nSiO_2(s) + 2\ HCl(g)$$

$$\Delta H_{1073K} = -5.71\ \text{kcal mol}^{-1} \text{ for } n = 1$$

is well known and has been studied.[8,9] The above reaction to form sodium silicates that are not readily soluble in water is believed to be the primary reaction for NaCl vapor retention by diatomaceous earth. Part of the NaCl vapor may also react with clays present as impurities in diatomaceous earth; clay minerals are known to be effective getters for alkali metal compounds.[10-12]

The solubility of an alkali metal silicate depends on the ratio of silica to alkali metal oxide and is also controlled by the amount of impurity present.[13] In an investigation of the kinetics of the above reaction, Chirkov[9,14] reported that at temperatures between 840 and 940°C, the rate of the above reaction increases with the temperature according to the Arrhenius equation. The rate of reaction of NaCl vapor with diatomaceous earth in the present system was also noted to increase with temperature, as noted in a previous report in this series, ANL/CEN/FE-78-10.

Bauxite is a principal ore of aluminum; it consists mainly of aluminum oxide and other impurities including SiO_2 and clay minerals. As shown and discussed in Section 1.c above, 51% of the NaCl vapor captured by fresh activated bauxite is captured by an adsorption process. In comparison with the chemical reactions of NaCl vapor with the SiO_2 and clay minerals in activated bauxite, the role played by an adsorption process sharply increases in later regeneration cycles.

e. Preliminary Economic Evaluations of Diatomaceous Earth and Activated Bauxite Used for the Removal of Alkali Metal Compounds from Hot Flue Gas of PFBC

The effectiveness of both diatomaceous earth and activated bauxite (alkali sorbents) for the removal of alkali metal compounds from hot simulated flue gas of PFBC has been experimentally demonstrated. The following is intended to further evaluate these two alkali sorbents from a practical economic point of view. To allow comparison, the cost of SO_2 sorbent is also included in this evaluation. Assumptions, computation bases, and part of calculated costs for all sorbents have been discussed in a previous quarterly report (ANL/CEN/FE-79-3).

It was assumed that a typical Illinois coal with a heating value of $29 \cdot 10^3$ J/g is combusted with 20% excess air, using Tymochtee dolomite at a Ca/S mole ratio of 1.5 for 80% sulfur removal. Costs were calculated of using diatomaceous earth or activated bauxite (on a once-through basis) as a bed material in a granular-bed filter to achieve removal of 97% of the alkalis from the hot flue gas generated from a 200-MWe demonstration plant having 40% over-all cycle efficiency. The calculated cost (Table 2) of using diatomaceous earth is about 1 mill per kW-h electricity produced. The cost of using activated bauxite is calculated to be about twice the cost of diatomaceous earth, but activated bauxite can be easily regenerated by a simple water-leaching process and recycled for reuse. Therefore, the cost of using activated bauxite, when calculated on the basis of regeneration, could be lower. This calculation will be made after more information is obtained about the water-leaching process.

Table 2. Evaluation of Cost of Granular Sorbents (1) for 97% Alkali Removal and (2) 80% Sulfur Removal for a 200-MWe PFBC Demonstration Plant

Sorbent	Cost Per kg Coal Burned, ¢	Cost Per kW-h Electricity Produced, mill
Diatomaceous Earth	0.31	0.96
Activated Bauxite	0.61	1.85
Tymochtee Dolomite	0.26	0.82

f. Future Work

Thus far, these two sorbents have been tested only at atmospheric pressure. In the actual application of a granular fixed-bed filter, the filter will be used at about 10-atm pressure. In order to test the sorbents for use in a pressurized system, a high-pressure sorption test unit is being set up. By use of this unit, the effects of pressure and the moisture content of the flue gas on the alkali vapor sorption performance of both diatomaceous earth and activated bauxite will be investigated; also, the pressure drop across the bed will be measured as a function of the superficial gas velocity. The regenerability (by water leaching) of activated bauxite after exposure to KCl and K_2SO_4 vapors will also be further studied.

2. Particle Removal from Flue Gas
(W. M. Swift, F. G. Teats, S. D. Smith, and J. J. Stockbar)

In PFBC, the hot flue gas from the combustor must be expanded through a gas turbine to recover energy and make the process economic. To prevent unacceptable erosion of the turbine blades by particles of limestone and fly ash entrained in the flue gas, the particle mass loading must be reduced to acceptable limits. Although the air quality requirements for gas turbines have not been agreed upon, estimates of acceptable mass loadings in the flue gas entering the turbine range from about 0.05 to 0.005 g/m^3,[15,16] depending on the particle size distribution.

There is considerable concern that at the high-temperature, high-pressure conditions of the flue gas between the combustor and the turbine, the very low loadings required by the turbine may not be achievable with existing particulate-control technology. It is necessary, therefore, that alternative and novel methods for the high-efficiency separation of solid particles from the high-temperature, high-pressure flue gas of a PFBC be investigated.

This report presents (1) a summary of the progress made in developing a pulse-jet/resonant manifold system for the investigation of acoustic dust conditioning and (2) the results of testing a high-efficiency cyclone.

a. Acoustic Dust Conditioning

Acoustic dust conditioning (ADC) is a technique to enhance the natural tendency of polydispersed particles to impact upon each other and agglomerate. Fine particle emissions are controlled in a process whereby the mean size of the effluent particles is significantly increased by exposure to high-intensity finite-amplitude acoustic fields. Acoustic dust conditioning would be incorporated into the off-gas treatment system to increase the collection efficiency of downstream dust collectors.

Efforts to develop and fabricate a pulse-jet acoustic dust conditioning (PJ-ADC) system were carried out under a subcontract at the University of Toronto.* Components of the acoustic generation system (see Fig. 5) include (1) a pulse-jet sound generator and (2) a resonant manifold system to match the acoustic system capacity with the FBC system volumetric gas flow capacity. A sound duct transmits sound into an acoustic treatment section where the flue gas can be exposed to the acoustic field.

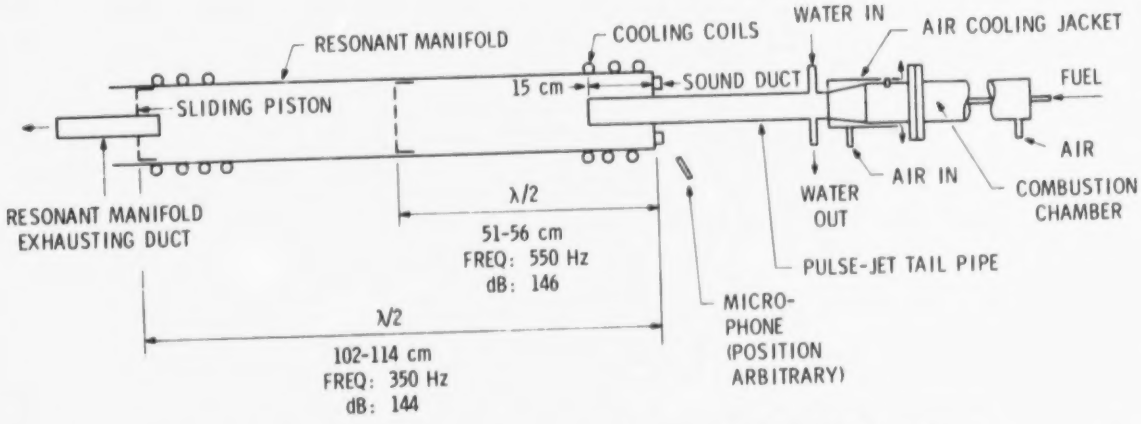

Fig. 5. Schematic of the Pulse-Jet/Resonant Manifold System

The merits of PJ-ADC as applied to PFBC have been reviewed,[17] and the basic reasoning in support of the development effort is repeated here:

1. PJ-ADC at ambient atmospheric conditions has achieved 5- to 7-fold increases in the mean particle diameter of industrial type aerosols.[18] Qualitative arguments (involving primarily interparticle spacing but not particle-particle adhesion) indicate that at the expected temperatures and pressures of PFBC, ADC should be even more effective than at ambient conditions.

*Direction was by Dr. David S. Scott, Professor and Chairman, Department of Mechanical Engineering.

2. Performance evaluations indicate that high-efficiency cyclones may reduce solids loadings sufficiently to meet the gas turbine inlet criterion for particle loading if the mean particle diameter entering the cyclone is increased by a factor of 2 to 5.[19]

3. Pulse jets are combustors, and exhausting the heat of combustion from pulse jets directly into the off-gases from PFBC would add to the internal energy of the flue gas. This heat would be extractable by the turbine with the same efficiency as the PFBC heat of combustion would be extracted from the flue gas. Thus, in principle, the power cost chargeable to particle gas separation by PJ-ADC would be very nearly zero.

4. Qualitative arguments indicate that pulse jets should yield more power and higher efficiencies when run at pressures greater than atmospheric.

5. The capital and operating costs for PJ-ADC are expected to be very low. Thus, the use of PJ-ADC could be very advantageous, whatever the particle/gas separation technology employed (high-efficiency cyclone, granular-bed filter, or ceramic fabric filter are examples).

The effort at the University of Toronto was scheduled to be completed in three phases: Phase I, which was completed, consisted of the design, fabrication, and testing of a pulse-jet resonant manifold system (PJ-RMS) at atmospheric pressure. Phase II, increasing the operating pressure of the PJ-RMS to about 1.01 MPa, was in progress when the project was temporarily discontinued for budgetary rather than technical factors. Phase III (the design, manufacture, and testing of a PJ-RMS system for installation and evaluation in the flue gas system of the ANL fluidized-bed combustion process development unit) was not initiated.

The results of the work performed at the University of Toronto were very encouraging technically. Major uncertainties surrounding the development of the PJ-RMS were removed, and the effort yielded no evidence that the technical objectives of the project could not be met. However, the project required significantly more developmental work than was originally anticipated. In the results summarized below, the advances made in pulse-jet technology during the developmental effort are emphasized.

Phase I. That Phase I was completed was signified by steady-state, continuous operation of a high-frequency, high-sound-intensity pulse jet exhausting into a tuned resonant manifold operating at approximately ambient conditions. Sound intensities as high as 160 dB were achieved while frequencies of about 300 Hz were maintained.

Prior to the initiation of this project, the University of Toronto had benefitted from the experience of developing pulse jets for ADC evaluations in various prototype projects conducted at Ontario Research Foundation.[18] However, the specific pulse jets used at Ontario Research Foundation were not well suited to the requirements of PFBC. To provide the necessary technical background for pulse-jet development as part of the ANL project, an extensive review of the literature was first undertaken.[20]

For reasons of safety and convenience, propane was selected as the fuel for the pulse jet during development. Although other fuels have not been used in the developmental program, almost any fuel can in principle can be adapted to pulse-jet operation--even pulverized coal.

The first PJ configurations examined in this study operated at sound intensities up to 130 dB and at frequencies up to 295 Hz, with the microphone placed at a relatively arbitrary location (at a 45° angle). In an intensive program of pulse-jet upgrading, units were developed which achieved sound intensities as high as 160 dB at a frequency of 280 Hz. During this development, dimensional and configurational changes were made in the combustion chamber, exhaust pipe, and air/fuel mixing and inlet designs. Furthermore, air- and water-cooling systems were developed for control of the metal temperatures of the combustion chamber and exhaust pipe, respectively.

After acceptable performance of the pulse jet was achieved, testing with the pulse jet exhausting into a resonant manifold was initiated. Tuned as a length resonator, the combined PJ-RMS exhibited the capability of producing greater total sound power, as well as higher frequencies, than could the same pulse jet exhausting into the free atmosphere. It was also discovered that a "double-frequency" operating mode could be achieved (at about 550 Hz) by proper adjustment of the overall length of the resonant manifold. At these "double frequencies," higher sound levels were achieved than with the normal RMS frequencies of about 300 Hz.

Although the absence of definitive and quantitative diagnostics prevents unequivocal claims to be made regarding pulse-jet performance, the following are claimed to be advances in pulse-jet technology:

1. The achievement of sound intensity levels of about 160 dB, as measured at the location indicated above, at a frequency of about 300 Hz is believed to exceed the highest sound levels previously obtained at this frequency by pulse jets.

2. A resonant manifold (length resonator) can be used to produce more total sound than can the pulse jet alone, and the frequency of the resonant-combustion can also be markedly increased by the addition of a resonant manifold.

Phase II. Phase II progress was evidenced by the successful operation of the PJ-RMS at pressures as high as 350 kPa. No operational difficulties were caused by these increased pressures. There is reason to believe that the increased fuel/air mass flow rates associated with increased operating pressure resulted in increased sound levels. Although operation of the pulse jet at 810 to 1015 kPa (the objective of the Phase II effort) is yet to be demonstrated, there is no reason to doubt that this can be achieved. Operation of the pulse jet at pressures significantly above atmospheric pressure constitutes another significant advance in pulse-jet technology.

Conclusions. On the basis of the developmental work at the University of Toronto, the feasibility of PJ-ADC for PFBC application continues to look technically feasible. The uncertainty regarding the feasibility of PJ operation at elevated pressures appears to be all but removed. Although the developmental work necessary to extend the operating characteristics of previously existing pulse-jet designs was significantly greater than anticipated, continued examination of PJ-ADC for high-temperature/high-pressure applications such as PFBC is warranted.

b. High-Efficiency Cyclone

A Donaldson Co. TAN-JET cyclone, claimed to have better dust-removal efficiency than conventional cyclones, was installed in the flue-gas system of the ANL 15.2-cm-dia combustor and has been undergoing testing and evaluation. The cyclone will also assist in the testing of the ANL granular-bed filter concept and possibly in future testing of acoustic dust conditioning as a concept for enhancing the particle-removal efficiency of separation devices.

Equipment. Figure 6 illustrates the current arrangement of the PDU-scale combustion test system. The combustor is a 15.2-cm-dia unit that can be operated at pressures between about 300 kPa and about 1000 kPa. Details of the combustor and ancillary equipment have been described in a previous report in this series (ANL/CEN/FE-78-10). As shown in Fig. 6, the TAN-JET is preceded in the flue gas system by a primary cyclone. In a few tests, the primary cyclone was removed from the system and the TAN-JET was operated as the system primary cyclone.

A conceptual schematic of the TAN-JET cyclone is shown in Fig. 7. The TAN-JET employs a secondary flow of clean air to provide a radial component of gas velocity in the primary dirty-gas flow. In Donaldson's design of the TAN-JET, the secondary air enters the cyclone through a multi-orificed nozzle at sonic velocity. Since sonic velocity is achieved at a pressure ratio of about 2 across a nozzle, the nozzle pressure drop has a design value of about 100 kPa, with the primary gas flow at atmospheric pressure.

The ratio of secondary air flow to total gas flow leaving the TAN-JET is controlled by the size and number of orifices in the secondary-air inlet nozzle. For ambient pressure operation, the nozzle flow rate was designed to be about 0.2 m^3/min at a nozzle Δp of about 103 kPa (15 psi) and a primary air flow of 2.5 m^3/min.

Figure 8 is a dimensional schematic of the TAN-JET cyclone; the actual and relative dimensions of the unit are given in Table 3. The relative dimensions of conventional cyclone designs are also given in Table 3 to allow comparison.

Although the TAN-JET received from Donaldson has a tangential inlet for the primary gas, Donaldson claims this is not essential to the performance characteristics of the cyclone.

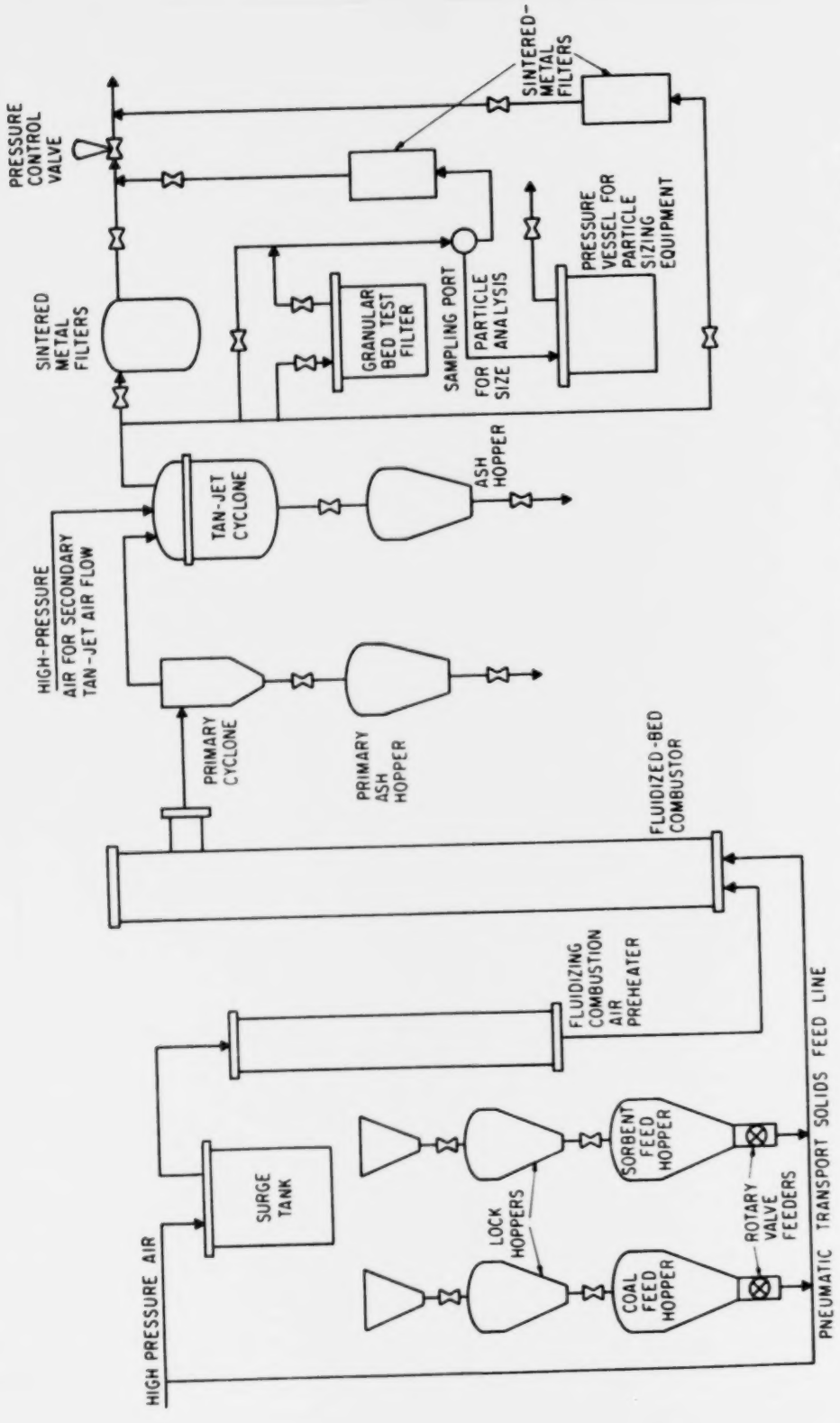

Fig. 6. Schematic Flowsheet of the Pressurized Fluidized-Bed Combustion System

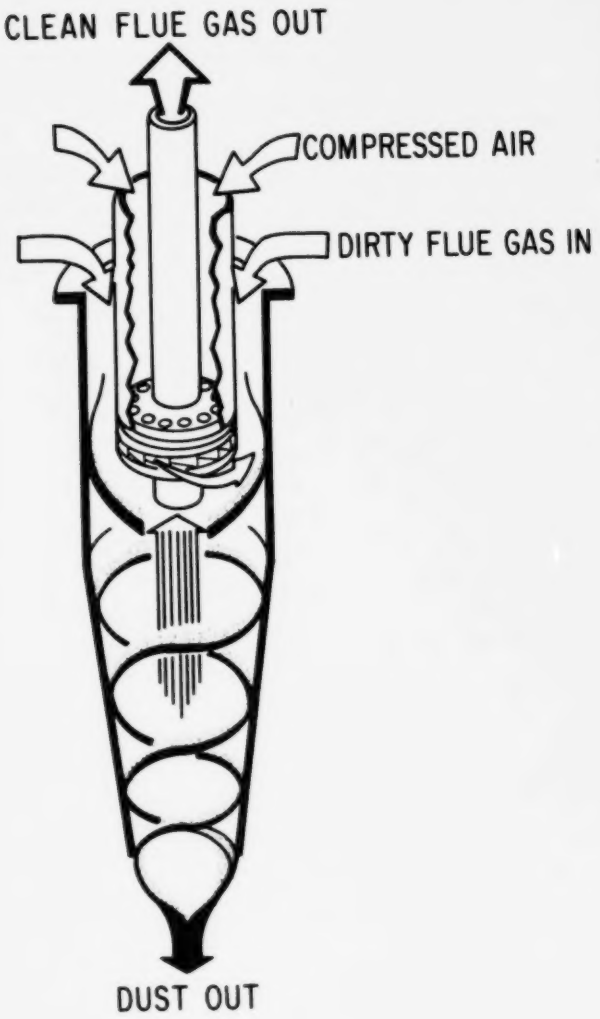

Fig. 7.

TAN-JET Tube

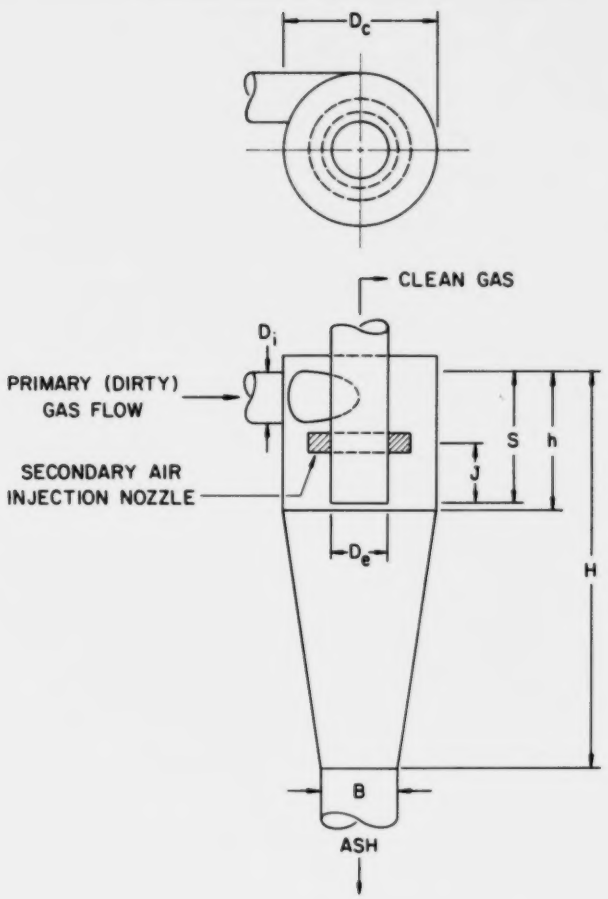

Fig. 8. Dimensional Schematic of the TAN-JET Cyclone (see Table 3 for nomenclature and dimensions)

Tests at Ambient Temperature. Initially, a series of experiments were performed in which a bed of limestone was fluidized in the combustor without coal combustion. The goal of the experiments was to observe the effect on TAN-JET cyclone performance of varying the pressure drop across the secondary air nozzle. In these experiments, the combustion system was pressurized to about 240-kPa absolute pressure. For the study, the high-pressure air supply to the secondary air nozzle was set at approximately 310, 345, or 380 kPa absolute for a pressure drop of 70, 105, or 140 kPa (10, 15, or 20 psi). To have obtained sonic velocity in the secondary air as it passed through the nozzle, a pressure drop of about 215 kPa (about 30 psi) would have been required at the system pressure of about 240 kPa (about 35 psia). Thus, the inlet gas velocities for the secondary air at the pressure drop levels of 70, 105, and 140 kPa were roughly 60, 70, and 80% of sonic velocity, respectively.

Table 3. Design Configuration of TAN-JET Cyclone and Other Cyclone Designs

Nomenclature (Refer to Fig. 8)	Dimensions				
	TAN-JET		Stairmond[a]	Swift[a]	Lapple[b]
	cm	Relative	(all relative dimensions)		
D_c, Body ID	14.3	1.00	1.0	1.0	1.0
D_i, Inlet ID[c]	5.2	0.36	(0.5 × 0.2)	(0.44 × 0.21)	(0.5 × 0.25)
S, Outlet Length	13.1	0.92	0.5	0.5	0.625
D_e, Outlet OD	5.7	0.40	0.5	0.4	0.5
h, Cylinder Height	13.8	0.96	1.5	1.4	2.0
H, Total Height	39.2	2.74	4.0	3.9	4.0
B, Dust Outlet ID	7.6	0.53	0.38	0.40	0.25
J, Sec. Air Inlet	6.0	0.42	N.A.[d]	N.A.	N.A.

[a]High-efficiency designs: C. Stairmond, Trans. Inst. Chem. Eng 29, 356 (1951); Steam Heating Engr. 38, 453 (1969).

[b]General-purpose design: C. E. Lapple, Air Pollution Engr. Manual (J. A. Danielson, Ed.), U.S. Dept. of Health, Education, and Welfare, Public Health Service Pub. No. 999,AP-40, p. 95 (1967).

[c]For conventional cyclones, dimensions are given for rectangular inlets; inlet height by inlet width.

[d]N.A. = not applicable.

In the experiments, a bed of fresh limestone in the combustor was fluidized at a superficial gas velocity of between 0.8 and 0.96 m/s, generating a dust-laden gas. Fresh limestone was continually fed to the combustor, and a constant bed height level was maintained *via* a 0.91-m-high overflow standpipe.

After steady operation during an experiment was established, the primary cyclone and TAN-JET cyclone hoppers were emptied and a timed period of solids collection was initiated. During this period, the flue gas downstream from the TAN-JET was sampled at the sampling port (see Fig. 6), using an Anderson cascade impactor. The efficiencies of the primary and TAN-JET cyclones were then calculated from the amounts of solids collected in their respective ash hoppers and from the solids loading downstream from the TAN-JET, as determined with the cascade impactor.

The results of the experiments are summarized in Table 4. Over the range of experimental conditions, the combined particle-collection efficiencies of the two cyclones were measured to vary between 96.4 and 99.5%, and particle loadings following the two stages of particle removal were 0.08 to 0.17 g/m^3.

Table 4. TAN-JET Cyclone Experiments at Ambient Temperature (System pressure: about 240 kPa absolute)

ΔP Across TAN-JET Secondary Air Nozzle, kPa	Expt. No.	TAN-JET Gas Flow Rates, m^3/min[a]		Particle Loading in Gas, g/m^3[a]			TAN-JET Primary Gas Flow Inlet Velocity, m/s	Particle Collection Efficiency, %		
		Primary	Secondary	Combustor Exit[b]	Primary Cyclone Exit[b]	TAN-JET Cyclone Exit[c]		Primary Cyclone	TAN-JET Cyclone	Combined
∿70	2	2.17	0.26	12	0.62	0.11	7.3	95	81	99.0
	6	2.38	0.26	17	1.1	0.17	7.8	94	82	98.9
∿105	1	2.21	0.33	5.0	0.29	0.08	7.4	94	69	98.1
	5	2.35	0.30	25	1.4	0.12	7.7	95	90	99.5
	9	2.66	0.34	13	0.69	0.13	8.6	95	79	99.0
∿140	3	2.19	0.36	2.3	0.34	0.08	7.4	86	74	96.4
	7	2.37	0.40	18	1.5	0.12	7.8	92	90	99.2
	10	2.66	0.38	12	1.2	0.14	8.6	90	86	98.6

[a]Measured at 21°C and 101 kPa absolute pressure.

[b]Based on primary gas flow.

[c]Based on total (primary plus secondary air) gas flow.

Examination of the data revealed that the only significant correlation in cyclone performance was the percent penetration of particulate matter through the cyclone as related to the mass loading in the flue gas entering the cyclone. This correlation is illustrated in Fig. 9. At an inlet mass loading of about 0.3 g/m^3, penetration was measured to be approximately 30%. At an inlet mass loading of about 1.5 g/m^3, penetration was measured to be only about 10%. (The wide variation in inlet loading was obtained when fluidizing two different limestones which had widely different attrition resistances.) In assessing the data, it is evident the tests were not sufficiently sensitive to detect the effects on collection efficiency of nozzle pressure drop or (2) minor variations in the primary gas inlet velocity to the TAN-JET. Penetration at a given inlet mass loading would be expected to decrease with increasing nozzle pressure drop (i.e., with increasing secondary gas flow rate and nozzle gas velocity) and with increasing primary gas inlet velocity.

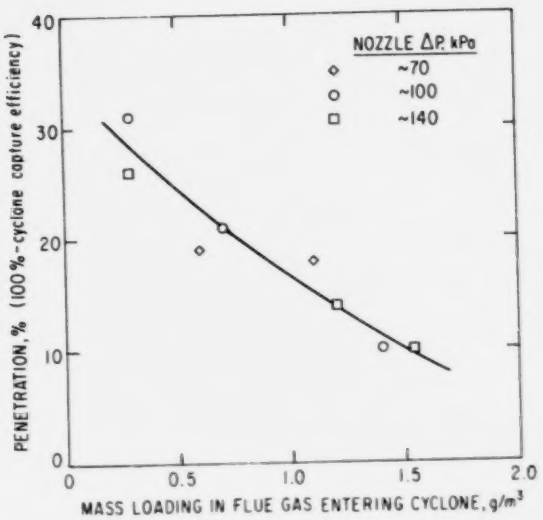

Fig. 9.

Penetration of Flue Gas Particulate Matter Through TAN-JET Cyclone as a Function of Mass Loading in Flue Gas Entering the Cyclone

The mass loadings in the flue gas leaving the TAN-JET were plotted (not shown) as a function of the mass loadings in the flue gas entering the cyclone. Although the data exhibit scatter, they do indicate (as expected) that despite the above-discussed increases in cyclone efficiency with increases in inlet mass loading, the outlet mass loadings increase at higher inlet mass loadings.

Tests at Elevated Temperature and 300-kPa Pressure. To extend the tests of the TAN-JET to conditions of higher inlet mass loadings, a series of experiments were performed at about 300-kPa system pressure and with coal burned in the combustor at 855°C. Particulate loadings in the flue gas leaving the combustor increased considerably (as compared with the tests at ambient temperature) due to carryover of fly ash and unburned carbon in addition to elutriated limestone. In these experiments, Sewickley coal was burned in a bed of Greer limestone sorbent with about 17% excess air and a fluidizing gas velocity of about 1.0 m/s.

Results of the tests are given in Table 5. In comparison with the results of the experiments at ambient temperature and about 240-kPa system pressure, the loadings of the gas leaving the primary cyclone and entering the TAN-JET were considerably higher. In these experiments, loadings to the TAN-JET ranged from approximately 1.8 to 3.4 g/m^3. In the ambient-temperature experiments, particle loadings ranged from approximately 0.3 to 1.5 g/m^3. With the higher loadings in the inlet stream, the TAN-JET collection efficiency ranged from a low of 88% to a high of 94%, and particle loadings in the outlet gas from the TAN-JET ranged from about 0.15 to 0.24 g/m^3.

To assess the effect of pressure drop across the secondary air inlet nozzle on cyclone efficiency, data from the ambient temperature experiments and the combustion experiments were analyzed as a single set of data. The combustion experiments were at a slightly higher pressure (305 kPa) than the ambient temperature experiments (240 kPa), and in the combustion experiments, the temperature of the primary gas flow entering the TAN-JET was nominally 250°C. The effects of the differences in operating conditions on TAN-JET cyclone efficiency were considered negligible compared with the effects of nozzle pressure drop and experimental error in making the determinations.

Figures 10, 11, and 12 illustrate, for secondary air nozzle pressure drop values of 70 kPa, 105 kPa, and 140 kPa, respectively, the effect of particle loading in the flue gas entering the TAN-JET cyclone on the penetration and the particle loading of the flue gas leaving the cyclone. The data points are those obtained both during the fluidization of limestone in the combustor at ambient temperature and 240 kPa and during the combustion of coal in a fluidized bed of limestone at 305 kPa (250°C flue gas temperature at the cyclone inlet).

Each set of data at a particular level of secondary air nozzle pressure drop was correlated using a power curve least squares fit of the form:

$$L_o = aL_i^b \qquad (1)$$

where

L_i is the inlet particle loading in g/m^3

L_o is the outlet particle loading in g/m^3

a and b are constants

Since penetration, P, is simply equal to $(L_o/L_i) \times 100\%$, the equation for the penetration correlation curve is:

$$P = 100\ aL_i^{(b-1.0)} \qquad (2)$$

The correlation equation and the coefficient of determination, r^2, for each correlation curve are also given in Figs. 10-12.

Table 5. Elevated-Temperature TAN-JET Cyclone Experiments (System pressure: ≃305 kPa absolute)

ΔP Across TAN-JET Secondary Air Nozzle, kPa	Expt. No.	TAN-JET Gas Flow Rates, m^3/min[a]		Particle Loading in Gas, g/m^3[a]			Particle Collection Efficiency, %		
		Primary	Secondary	Combustor Exit[b]	Primary Cyclone Exit[b]	TAN-JET Cyclone Exit[c]	Primary Cyclone	TAN-JET Cyclone	Combined
∿70	LP1E-1	0.856	0.185	30.5	2.10	0.20	93.1	88.6	99.2
	LP1E-2	0.847	0.186	29.2	3.35	0.24	88.5	91.2	99.0
∿105	LP1B	0.865	0.236	34.9	3.02	0.15	91.4	93.6	99.4
	LP1D-1	0.862	0.234	38.2	3.13	0.15	91.8	94.0	99.5
	LP1D-2	0.858	0.229	35.8	2.61	0.15	92.7	92.8	99.5
∿140	LP1F	0.853	0.259	31.6	3.15	0.15	90.0	93.9	99.4
	LP2A	0.859	0.263	33.0	1.75	0.12	94.7	90.8	99.5

[a]Measured at 21°C and 101 kPa absolute pressure.

[b]Based on primary gas flow.

[c]Based on total (primary plus secondary air) gas flow.

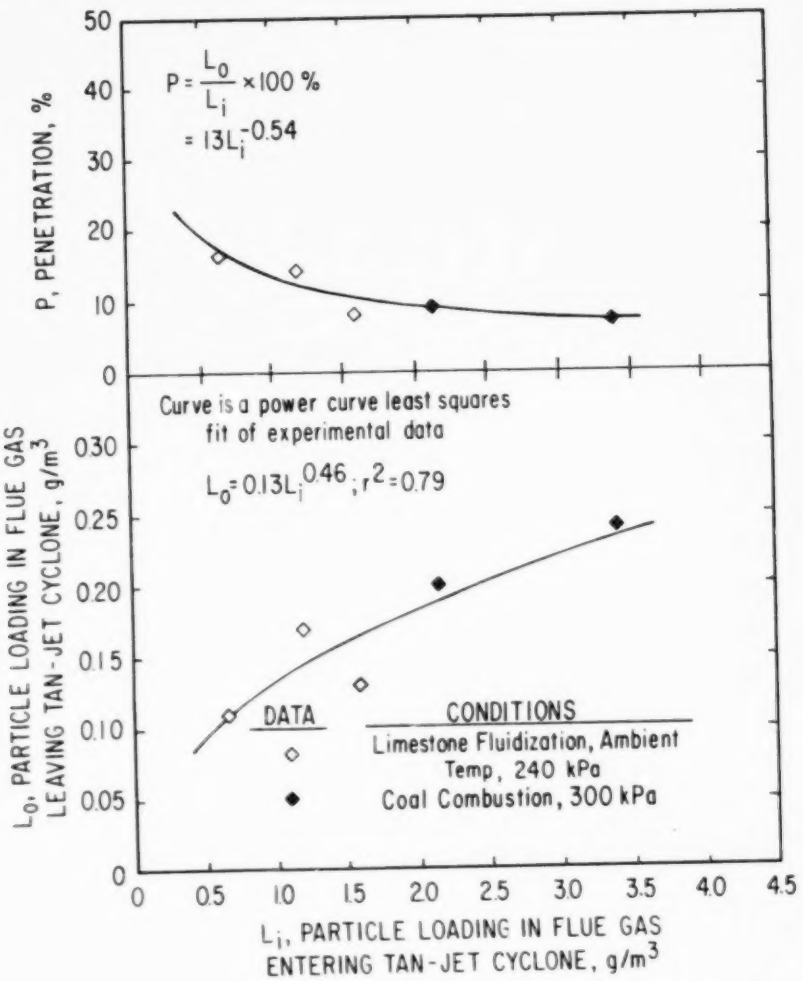

Fig. 10. Penetration and Particle Loading in Flue Gas Leaving TAN-JET Cyclone as a Function of Particle Loading Entering TAN-JET Cyclone for Secondary Air Nozzle. $\Delta P \cong 70$ kPa.

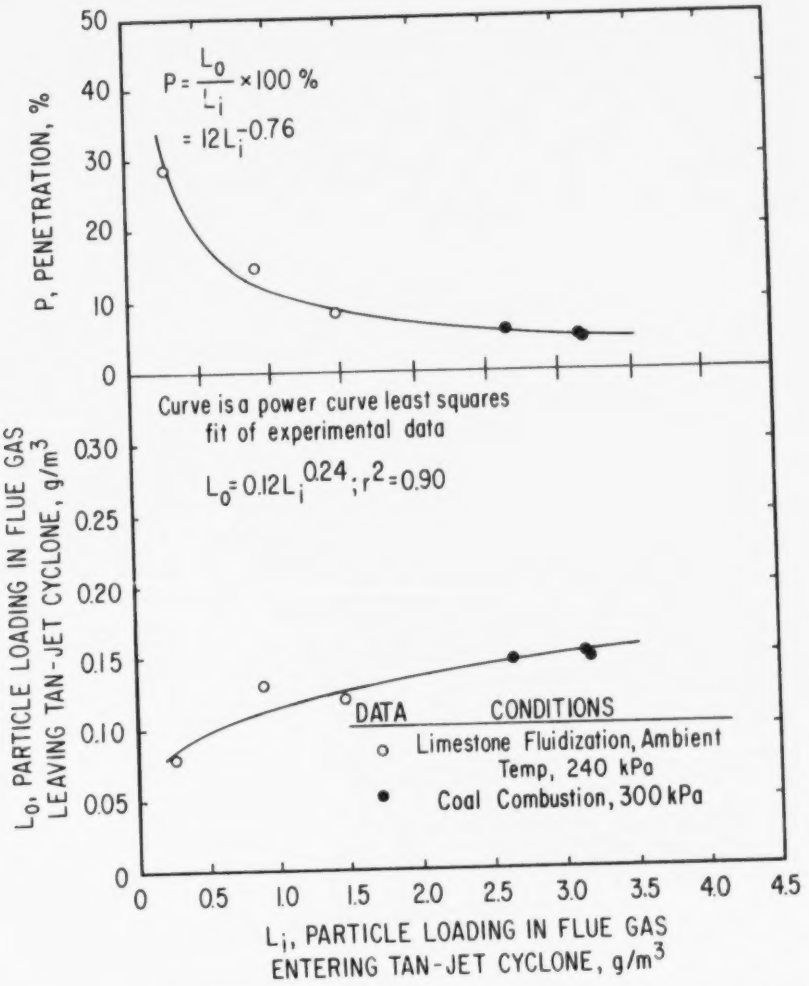

Fig. 11. Penetration and Particle Loading in Flue Gas Leaving TAN-JET Cyclone as a Function of Particle Loading Entering TAN-JET Cyclone for Secondary Air Nozzle. $\Delta P \cong 105$ kPa.

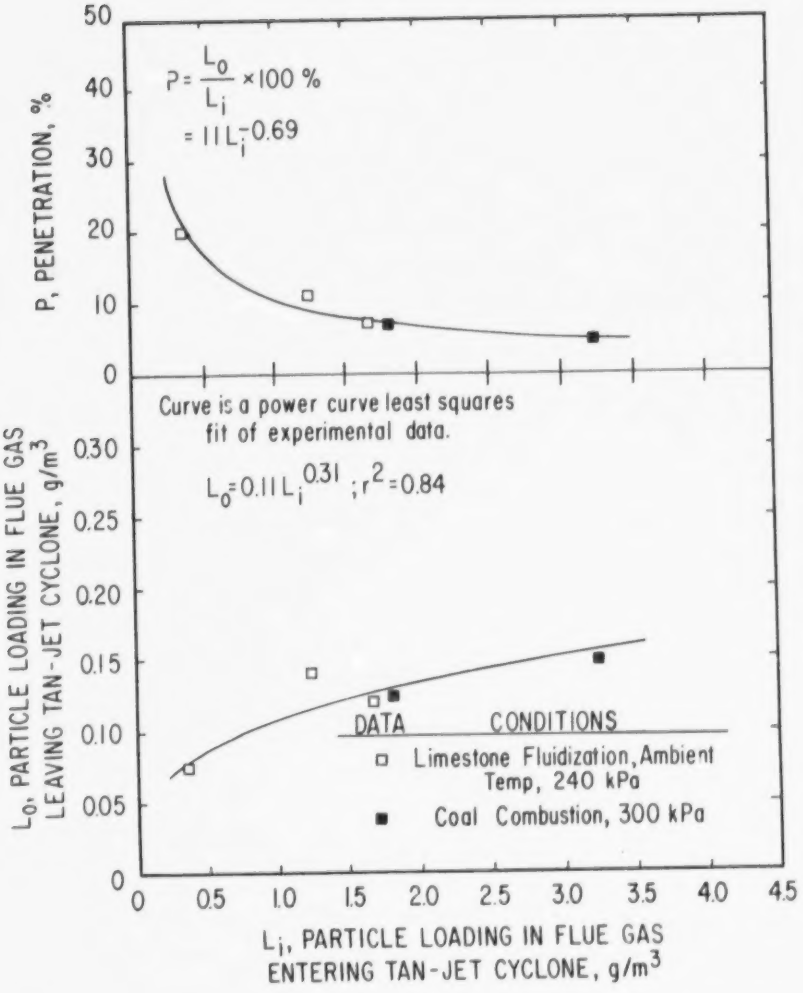

Fig. 12. Penetration and Particle Loading in Flue Gas Leaving TAN-JET Cyclone as a Function of Particle Loading Entering TAN-JET Cyclone for Secondary Air Nozzle. $\Delta P \cong 140$ kPa.

The correlation curves for the experimental results at nozzle pressure drops of 105 kPa and 140 kPa are very similar, indicating that nozzle pressure drop has little or no effect above a certain minimum value. At the lowest nozzle pressure drop tested (70 kPa), the level of particle penetration and the resulting mass loading in the flue gas leaving the TAN-JET were considerably greater than at the greater nozzle pressure drop levels. This difference is only apparent, however, at the higher inlet mass loadings encountered in the second set of experiments with coal combusted in the combustor.

Tests at Elevated Temperature and 810-kPa Pressure. Results of a number of experiments in which coal was combusted in a fluidized-bed of dolomite at a system pressure of 810 kPa and a bed temperature of 870°C were analyzed to evaluate the performance of the TAN-JET at high pressure.

The experimental conditions and results of the high-pressure TAN-JET performance tests are presented in Table 6. The test results given in Table 6 represent approximately two-thirds of the tests in which TAN-JET performance data were collected. The complete set of experimental results exhibited an unreasonable degree of scatter. In an attempt to clarify the results, the measurements of dust loading in the flue gas leaving the combustor, the primary cyclone, and the TAN-JET in each experiment in the test series were examined. If a measured value for any parameter was highly inconsistent in comparison to measured values in replicate experiments (i.e., if there was a factor-of-two difference or greater), all measured values for that experiment were considered suspect and were rejected. Approximately one-third of the results of experimental tests were rejected in this manner.

"Erroneous" readings are most likely to be caused by irregular discharge of ash from the primary and TAN-JET cyclones, possibly a result of occasional temporary plugging in the ash discharge lines. The cyclone efficiency values are highly dependent on the weights of timed ash dumps from the cyclone hoppers and thus are sensitive to variations in the ash discharge rate.

Figure 13 illustrates the loadings in the flue gas leaving the combustor (operated at 810 kPa and 850°C bed temperature) at the three levels of fluidizing gas velocity used for the experiments. The loadings were indirectly determined from the timed rates of solids removal from the primary cyclone and secondary cyclone (TAN-JET) plus the measured solids loadings in the flue gas downstream from the TAN-JET.

The loadings increased from approximately 17 g/m^3 at a nominal combustion gas velocity of 0.6 m/s to approximately 32 g/m^3 at a nominal combustor gas velocity of 1.4 m/s. The high loadings are the result of the decrepitation of the particular stone used in these experiments (a dolomite which has a relatively high decrepitation tendency).

The particle-removal characteristics of the primary cyclone were also determined, with the results correlated with the particle loading of the gas entering the primary cyclone and the volumetric gas flow through the cyclone. The data are presented in Figs. 14 and 15. Both Figs. 14 and 15

Table 6. Elevated-Temperature TAN-JET Cyclone Experiments (System pressure: ~810 kPa absolute)

ΔP Across TAN-JET Secondary Air Nozzle, kPa	Expt. No.	TAN-JET Gas Flow Rate, m^3/min[a]		Nominal Combustor Gas Velocity, m/s	Particle Loading in Flue Gas, g/m^3[a]			Particle Collection Efficiency, %		
		Primary	Secondary		Combustor Exit[b]	Primary Cyclone Exit[b]	TAN-JET Cyclone Exit[c]	Primary Cyclone	TAN-JET Cyclone	Combined
70	1E-1	2.29	0.35	1.0	24.7	2.25	0.19	90.8	90.1	99.1
70	1E-2	2.29	0.32	1.0	23.4	1.74	0.24	92.5	84.0	98.8
70	1L-1	2.29	0.29	1.0	26.8	1.20	0.29	95.5	72.7	98.8
70	1Y-2	3.24	0.31	1.4	30.2	4.83	0.59	84.0	86.5	97.8
105	1O-1	1.33	0.38	0.6	15.0	0.95	0.15	93.7	79.4	98.7
105	1P-1	1.33	0.37	0.6	17.9	1.93	0.16	89.2	89.5	98.9
105	1U-1	1.33	0.36	0.6	17.7	1.51	0.09	91.5	92.1	99.3
105	1U-2	1.33	0.36	0.6	17.7	1.51	0.09	91.5	92.1	99.3
105	1H-1	2.32	0.41	1.0	25.4	1.69	0.17	93.3	88.0	99.2
105	1H-2	2.32	0.41	1.0	26.2	1.65	0.12	93.7	91.1	99.4
105	1Q-2	2.24	0.35	1.0	29.4	1.48	0.20	95.0	84.4	99.2
105	1T-1	2.23	0.36	1.0	27.3	1.43	0.13	94.7	89.1	99.4
105	1T-2	2.23	0.36	1.0	27.2	1.40	0.11	94.8	90.9	99.5
105	2	2.23	0.28	1.0	24.0	1.29	0.15	94.6	86.8	99.3
105	2A	2.24	0.32	1.0	23.3	1.59	0.12	93.2	91.0	99.4
105	1Z-1	3.26	0.33	1.4	33.2	5.70	0.36	82.8	93.1	98.8
105	1Z-2	3.23	0.32	1.4	33.6	5.90	0.50	82.5	90.6	98.4
140	1X-1	3.17	0.32	1.4	30.3	3.68	0.23	87.8	93.2	99.2
140	1X-2	3.14	0.32	1.4	30.5	3.61	0.14	88.1	95.9	99.5

[a]Measured at 21°C and 101 kPa absolute pressure.

[b]Based on primary air volumetric flow rate.

[c]Based on total (primary plus secondary) air volumetric flow rate.

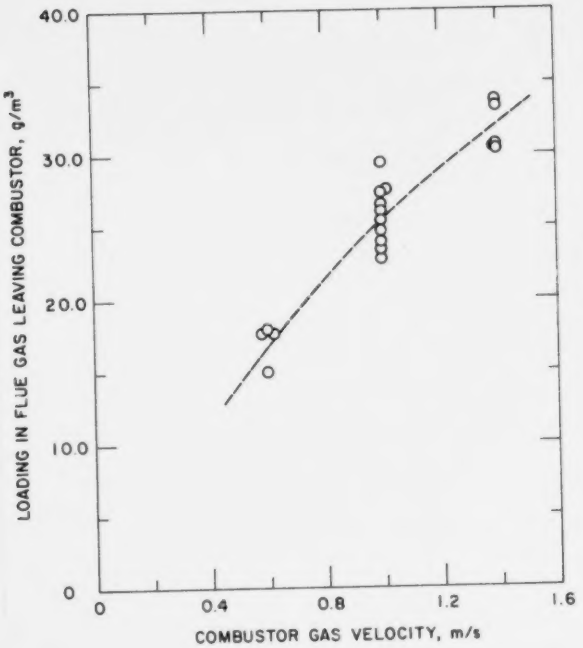

Fig. 13.

Particle Loadings in Flue Gas Leaving the PDU Combustor during Operation at 810 kPa and 875°C

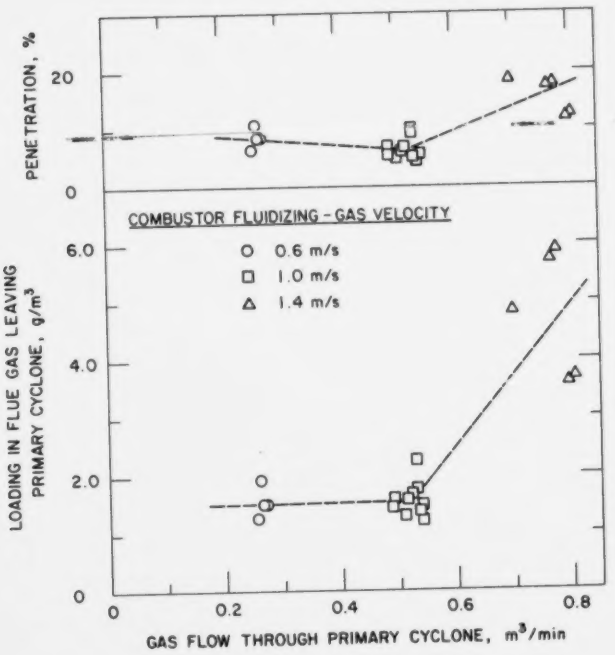

Fig. 14. Primary Cyclone Performance Related to Solids Loading in Flue Gas Entering the Cyclone

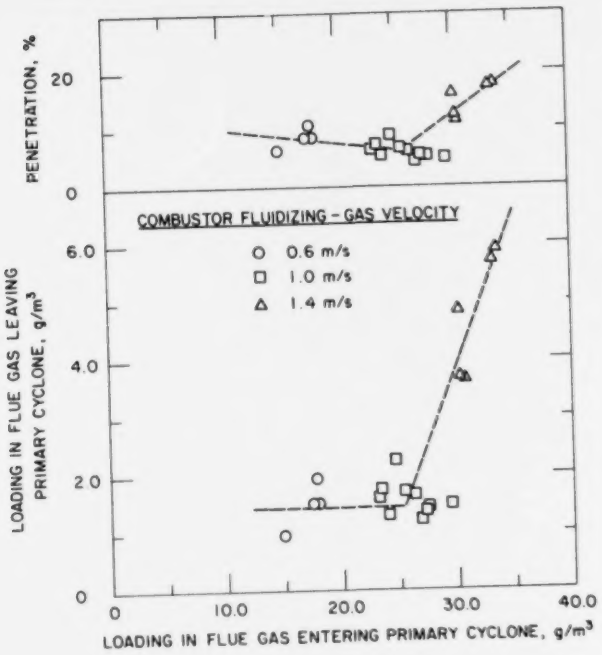

Fig. 15. Primary Cyclone Performance Related to Gas Flow Through the Cyclone

illustrate that the particle loading of gas leaving the primary cyclone and the mass penetration of the cyclone (100% - particle collection efficiency) were fairly stable except in experiments at a combustor gas velocity of 1.4 m/s. Thus, it appears that at the highest combustor gas velocity, the gas flow through the primary cyclone (0.7 m^3/min or greater) exceeded the capacity of the cyclone so that particle reentrainment was occurring. At the lower gas flows through the cyclone, approximately 0.5 and 0.25 m^3/min, penetration was about 5 to 10% and particle loadings were about 1.5 g/m^3.

The particle-removal capability of the TAN-JET cyclone in the 810-kPa system pressure experiments is illustrated in Figs. 16 and 17. As for the primary cyclone, the TAN-JET data are reported as percent mass penetration and as particle loading in the flue gas leaving the cyclone as functions of the inlet mass loading and the total (primary plus secondary) volumetric flow rate through the unit.

Figure 17 gives the clearest impression of the influence of the secondary air on cyclone performance. At the medium and high gas throughputs of 0.6 and about 0.85 m^3/min, the influence of the nozzle ΔP on cyclone performance is evident, i.e., the loading in the flue gas and the percent penetration decrease as the nozzle ΔP increases.

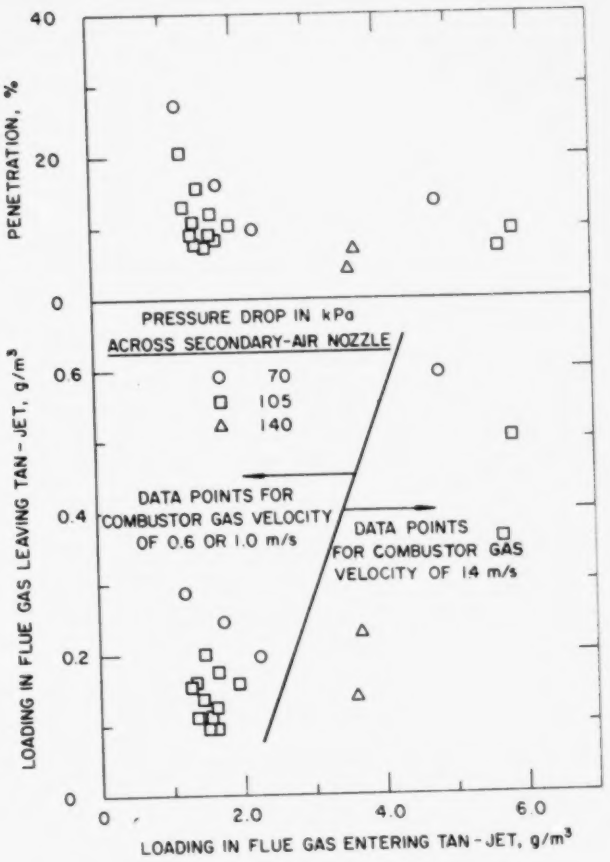

Fig. 16. TAN-JET Cyclone Performance Related to Solids Loading in Flue Gas Entering the Cyclone

The dramatic increase in particle loadings leaving the TAN-JET at the highest gas throughput is undoubtedly related to the inlet loadings being significantly greater at this gas flow by a factor of 2 to 3 than at the two lower gas flows (see Fig. 16). This dramatic shift in the loading of the inlet gas at the higher gas throughput evidently resulted from exceeding the capacity of the primary cyclone.

A qualitative comparison of TAN-JET performance with coal combustion at 810-kPa and 300-kPa system pressures is quite interesting. For experiments at a gas velocity of 1 m/s in the fluidized bed (about 0.6 m^3/min flow through the TAN-JET), inlet loadings to the TAN-JET during the high-pressure tests were generally between 1.0 and 2.0 g/m^3 (Fig. 16). At the above conditions with secondary air nozzle pressure drops of 70 and 105 kPa, respectively, outlet loadings ranged from about 0.2 to 0.3 g/m^3 and from about 0.1 to 0.2 g/m^3. As seen in Fig. 10, at the lower pressure conditions with an inlet loading of between 1 and 2 g/m^3 and a nozzle ΔP of 70 kPa, outlet loadings taken from the correlation are in the range of 0.13 to 0.18 g/m^3,

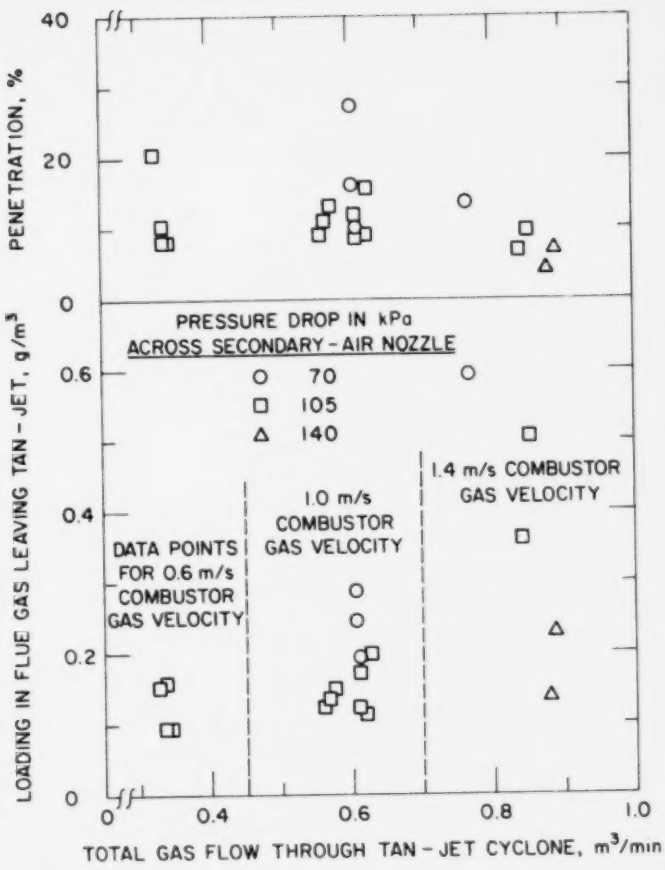

Fig. 17. TAN-JET Cyclone Performance Related to Gas Flow Through the Cyclone

which are approximately 30% lower than in the experiments at 810 kPa. At a nozzle ΔP of 105 kPa for the lower pressure experiments (Fig. 11), outlet loadings in the range of 0.12 to 0.14 g/m^3 are projected for inlet loadings of 1 to 2 g/m^3, values which fall within the lower end of the range of values observed in the experiments at 810 kPa.

The above result, i.e., a decrease in cyclone performance with an increase in system pressure for a given level of nozzle pressure drop, is obtained consistently. As the system pressure is increased, a higher nozzle ΔP is required to achieve the same velocity of the secondary air passing through the air nozzle. Thus, at a system pressure of 300 kPa and a nozzle ΔP of 105 kPa, the secondary air velocity is about 63% of sonic. At 810 kPa and a nozzle ΔP of 105 kPa, the secondary air velocity is only about 38% of sonic. An additional simple analysis also shows that at the conditions compared here, the kinetic energy of the secondary air entering the TAN-JET at 810-kPa system pressure and 105-kPa pressure drop is only about 60% of the kinetic energy of the secondary air at 300-kPa system pressure and 105-kPa pressure drop.

TAN-JET Performance Tests as Primary Cyclone. A separate test series of four experiments was performed at 810-kPa system pressure with the primary cyclone removed from the flue gas system and the TAN-JET cyclone accepting the full loading of the flue gas leaving the combustor. In the experiments carried out during the combustion of coal, the nozzle ΔP was varied in a stepwise manner from about 70 kPa to about 105 kPa. At each level of nozzle ΔP, the loading in the flue gas leaving the cyclone was measured by passing a small, metered slipstream of the total gas flow (obtained using an iso-kinetic probe) through a Gelman filter. The conditions and results of the experiments are given in Table 7 and Fig. 18.

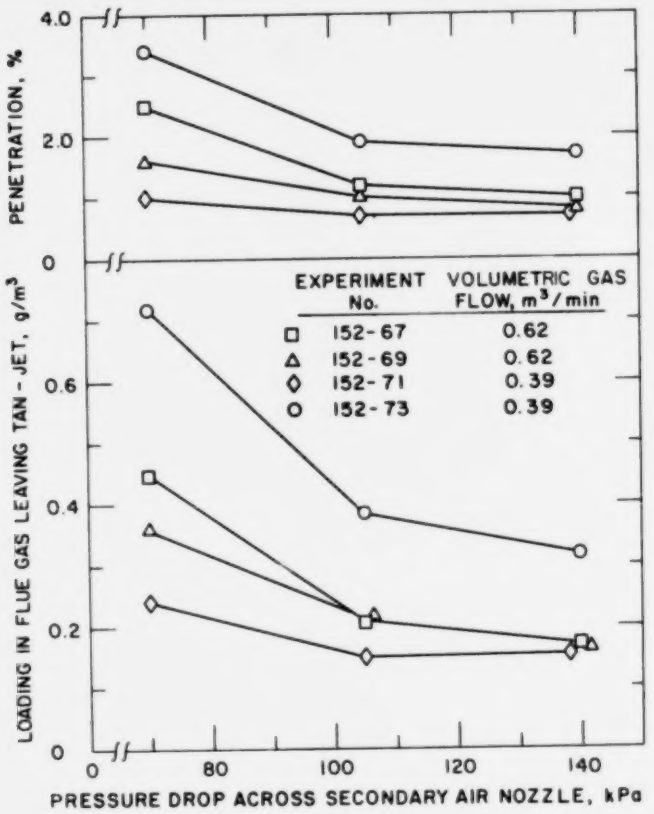

Fig. 18. TAN-JET Performance Characteristics as a Function of Secondary Air Nozzle Pressure Drop with TAN-JET as Primary Cyclone. Gas flow in key given in actual cubic meters per minute.

Table 7. Conditions and Results of Experiments with TAN-JET as the Primary Cyclone

Coal: Sewickley — Temperature: 875°C

Limestone: Vulcan dolomite — Pressure: 810 kPa

Expt.	ΔP Across TAN-JET Secondary Air Nozzle, kPa	TAN-JET Gas Flow Rate, m^3/min[a]		Particle Loading in Flue Gas, g/m^3[a]		Particle Collection Efficiency, %	Penetration, %
		Primary	Secondary	Combustor Exit[b]	TAN-JET Exit[c]		
152-67-1	70	2.24	0.29	20.3	0.44	97.5	2.5
-2	105	2.24	0.36	20.0	0.20	98.8	1.2
-3	140	2.24	0.43	20.0	0.17	99.0	1.0
152-69-1	70	2.24	0.29	26.2	0.36	98.4	1.6
-2	105	2.24	0.37	26.0	0.21	99.0	1.0
-3	140	2.24	0.46	26.0	0.17	99.2	0.8
152-71-1	70	1.33	0.29	28.9	0.24	99.0	1.0
-2	105	1.33	0.36	28.8	0.15	99.3	0.7
-3	140	1.33	0.42	28.8	0.15	99.3	0.7
152-73-1	70	1.33	0.29	25.6	0.72	96.6	3.4
-2	105	1.33	0.36	25.2	0.38	98.1	1.9
-3	140	1.33	0.42	25.1	0.32	98.3	1.7

[a]Measured at 21°C, 101-kPa pressure.

[b]Based on primary air volumetric flow rate.

[c]Based on total (primary plus secondary) air volumetric flow rate.

The results rather dramatically illustrate the influence of the nozzle ΔP on cyclone performance. In each experiment, the measured loading in the flue gas leaving the TAN-JET decreased as the nozzle ΔP was increased from 70 to 105 to 140 kPa. With the exception of Expt. 152-73 (data represented by circles in Fig. 19) for which the data are unexplainably inconsistent with data for the other tests, penetration at a nozzle ΔP of 140 kPa was between 0.7 and 1.0% and the loading in the flue gas leaving the TAN-JET was 0.15 to 0.17 g/m^3.

When the results of the tests using the TAN-JET alone (but excluding Expt. 152-73) are compared with the results of the tests using the primary cyclone plus the TAN-JET (Table 6), little loss in performance was noted in using the TAN-JET alone. At a nozzle ΔP of 105 kPa, collection efficiency using the TAN-JET alone was 98.8 to 99.3%. The combined or overall collection efficiency when using both cyclones under similar conditions was 98.4 to 99.5%. At a nozzle ΔP of 140 kPa, collection efficiency with the TAN-JET alone was between 99.0 and 99.3% and in two tests with both cyclones operating was either 99.2 or 99.5%.

Particle Size Selectivity of TAN-JET Cyclone. Attempts have been made in two experiments to determine the size selectivity of the TAN-JET (i.e., the cyclone efficiency as a function of incoming particle size). The two experiments were: (1) Expt. LP1D-1 performed at 305-kPa system pressure (see Table 5), and (2) Expt. 1T-1 performed at 810-kPa system pressure (see Table 6). In those experiments, samples of (1) the fly ash collected in the TAN-JET ash receiver and (2) fly ash filtered from the flue gas downstream from the TAN-JET cyclone were sent to independent laboratories (A and B) for particle size analysis. The analyses were performed using Coulter counters.

The results of the particle size determinations are shown in Figs. 19 and 20. Figure 19 illustrates the reported particle size distributions of the ash recovered in the TAN-JET hopper for both experiments. It should be noted that Experiment 1T-1 was a high-pressure (810-kPa) combustion run using a dolomite sorbent. Experiment LP1D-1 was a lower-pressure (305-kPa) experiment using a limestone sorbent. Therefore, the distributions of the ash material in the TAN-JET hopper could reasonably be expected to differ considerably in the two experiments.

It should also be noted that a third laboratory performed analyses of the same samples whose distributions are presented in Figs. 19-20. The results reported by that laboratory, however, were highly suspect since (1) they showed evidence of internal inconsistencies (highly irregular distributions) and (2) they indicated mass mean diameters that were considerably greater (by an order of magnitude) than those reported by the other laboratories. It is suspected that inadequate redispersion of the samples in the electrolyte used for the Coulter counter analysis was responsible. Hence, the results from that laboratory have not been presented here.

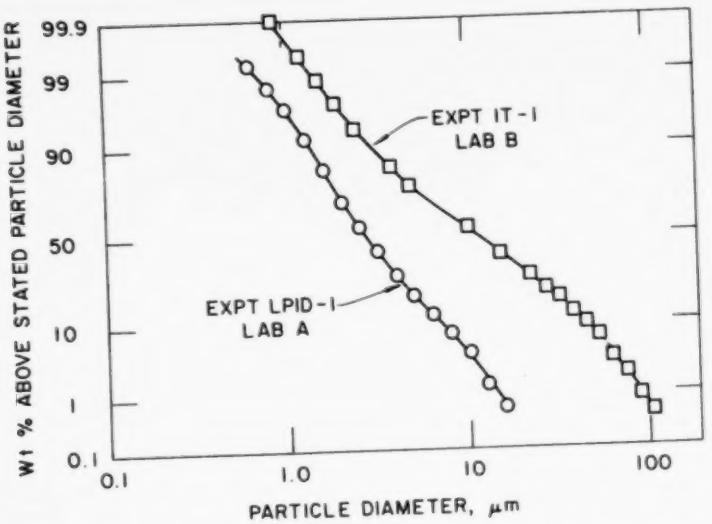

Fig. 19. Particle Size Distributions of Fly Ash Recovered from TAN-JET Cyclone Hopper

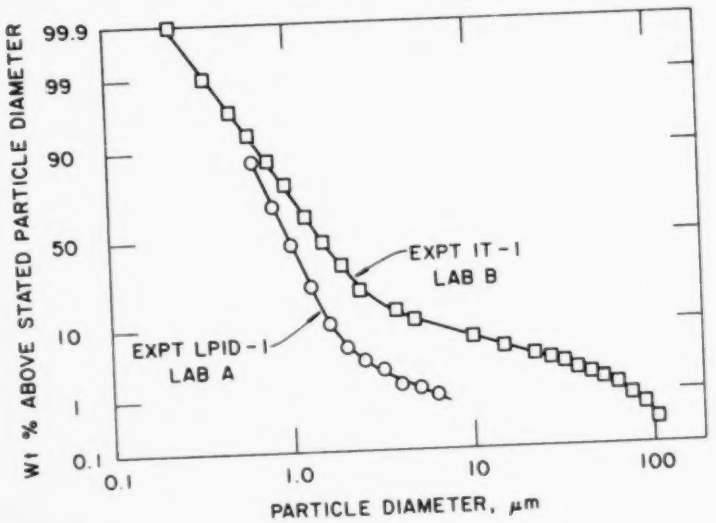

Fig. 20. Particle Size Distributions for Samples of Fly Ash Filtered from Flue Gas Downstream from TAN-JET Cyclone

The mass mean particle diameter of the hopper ash as indicated in Fig. 19 is about 11 μm for the sample from the high-pressure experiment and about 2.7 μm for the sample from the low-pressure experiment.

Figure 20 presents the particle size distributions for the samples of fly ash filtered from the flue gas downstream from the TAN-JET cyclone. The distributions reported by Laboratories A and B for the samples from the separate experiments show a fairly high degree of similarity. Laboratory A reported a mass mean diameter of 1.0 μm for the low-pressure experiment sample, Laboratory C a mass mean diameter of about 1.5 μm for the high-pressure experiment sample.

Using the distributions of Fig. 20, the measured particle loadings downstream from the TAN-JET for the two combustion experiments have been broken down into particle size ranges (Table 8).

Table 8. Particle Loading Downstream from TAN-JET by Particle Size Range

Experiment No.	Particle Mass Loading in Indicated Particle Size Range, $(g/m^3)/(grains/scf)$			
	<2 μm	2-10 μm	>10 μm	Total
LP1D-1 (3 atm)	(0.27)/(0.12)	(0.018)/(0.008)	0	(0.29)/(0.13)
1T-1 (8 atm)	(0.091)/(0.040)	(0.034)/(0.015)	(0.009)/(0.004)	(0.13)/(0.059)

In both cases, the major contribution to the total loading is from particles smaller than 2 μm in diameter. These particles are not believed to be of significant concern in affecting turbine erosion though particles smaller than 2 μm may pose a potential problem of turbine fouling and corrosion as a result of particle deposition on the turbine blades. Particles larger than 10 μm, which are of serious concern because of their erosion potential, are present in very small amounts (<0.01 g/m^3).

The particle loading conditions in the flue gas leaving the TAN-JET for these two experiments can also be compared with conditions estimated to be acceptable for a gas turbine. The results are illustrated in Fig. 21. In the case of the data from the 810-kPa experiment, the total loading starts out at a moderately high 0.06 grains/scf (about 0.13 g/m^3), and the cumulative loading (loading greater than corresponding particle diameter) decreases rapidly with increasing particle diameter until about 10 μm, at which point the curve tends to decrease much less rapidly. The particle sizes in this experiment exceed those which workers at Westinghouse[15] (Ⓦ) and General Electric[16] (GE) estimated to be acceptable for a gas stream entering a gas turbine.

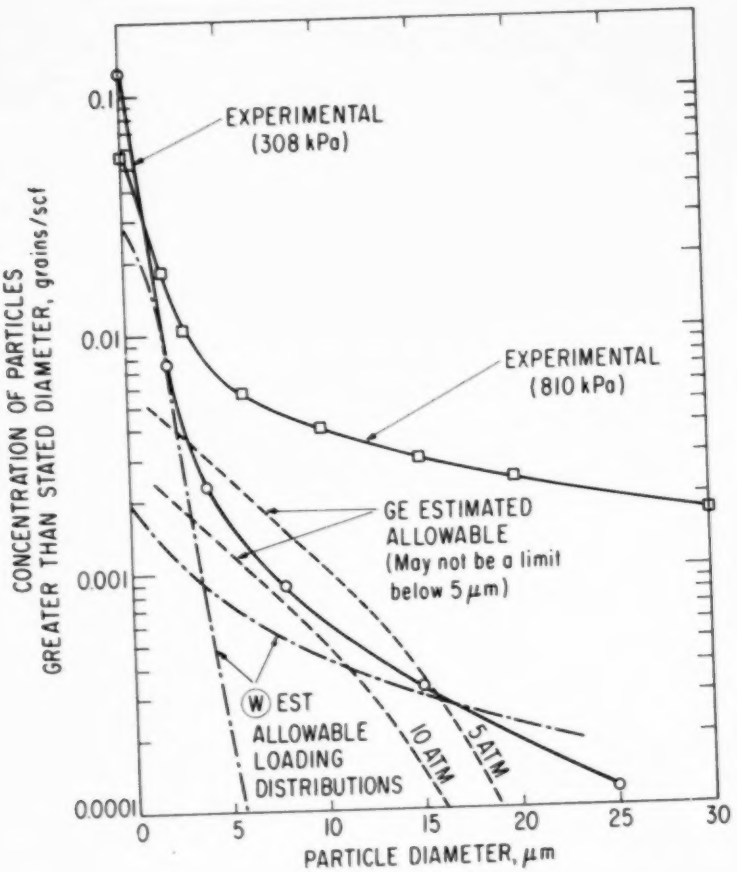

Fig. 21. Comparison of Concentrations of Particles in Flue Gas Leaving TAN-JET Cyclone as a Function of Particle Diameter, Along with Estimates of Acceptable Distributions for Gas Turbines

The results for the 305-kPa experiment are somewhat more encouraging. Although the total loading is a very high, 0.12 grains/scf (0.29 g/m^3), the experimental cumulative loading curve at points beyond about 3 μm does fall within the range of concentrations estimated to be acceptable. Additional data are required, however, to determine which of the two experimental loading distributions is more representative of the TAN-JET performance. The variance in results cannot be fully explained on the basis of the difference in system pressure for the two experiments.

Figure 22 presents the distributions of the fly ash entering the TAN-JET cyclone as constructed from the respective particle size distributions given in Figs. 19 and 20, together with the measured TAN-JET ash collection rates and downstream loadings. Since the cyclone is highly efficient, the inlet mass distributions closely resemble the distributions of the samples

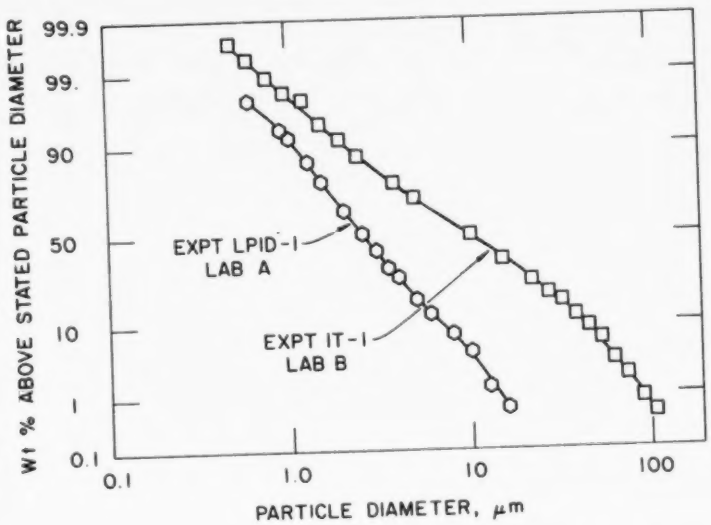

Fig. 22. Calculated Particle Size Distributions of Dust Entering TAN-JET Cyclone

collected in the cyclone hopper. The mass mean diameters of the inlet distributions as constructed in Fig. 22 are 2.5 μm for the low-pressure experiment and 10 μm for the high-pressure experiment.

Using the distribution data, grade efficiency curves were calculated for both experiments and are presented in Fig. 23, along with a grade efficiency curve provided by the cyclone manufacturer. For the low-pressure experiment, the performance curve is significantly better than was anticipated for the unit. The result for the high-pressure experiment agrees fairly well with the vendor-supplied curve. Indicated cut points for the cyclone (the size of a particle removed with 50% efficiency) are about 0.9 μm for the low-pressure experimental data, about 1.6 μm for the high-pressure data, and about 2.0 μm for the vendor-supplied curve. The results are quite encouraging in that the unit exhibits a very high particle removal efficiency for particles as small as 2 μm.

Future Work. Additional experiments are planned to further quantify the grade efficiency performance of the TAN-JET and to assess the effect of operating conditions on that performance characteristic.

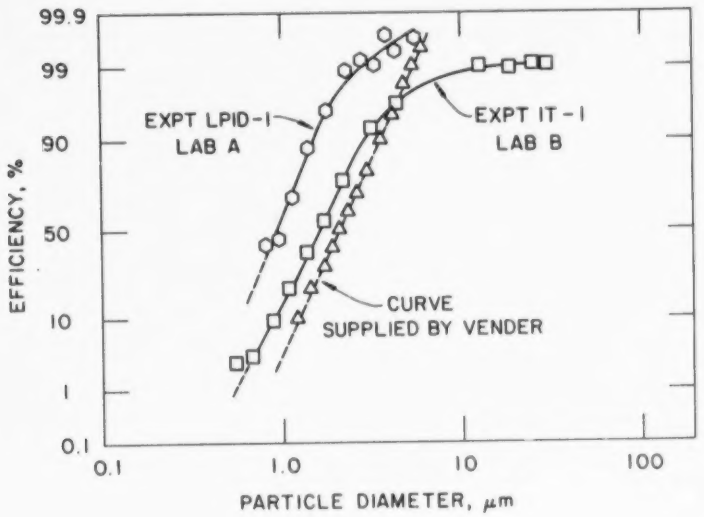

Fig. 23. Calculated Grade Efficiency Curves for TAN-JET Cyclone

TASK B. TRACE POLLUTANTS IN THE FLUIDIZED-BED COMBUSTION OF COAL
(A. A. Siczek and K. M. Myles)

The objective of this program is to develop methods of reducing the potential environmental pollution of trace organic compounds and inorganic elements released during the fluidized-bed combustion of coal. Most of the previous work on air pollution control of the FBC has been focused on emission of SO_x, NO_x, and respirable particulates, since they contribute the greatest concentration of material emitted to the atmosphere. The trace pollutants under consideration can be grouped into three categories, and each will be discussed separately: (1) organic compounds, (2) inorganic elements, and (3) radioactive isotopes. The pollutants are either originally present in the coal or formed during the combustion process. The pollutants are released to the environment by both off-gas emission and ash disposal.

Organic pollutants originate from either the incomplete combustion of coal or are products of the chemical reactions taking place in both reducing and oxidizing atmospheres of the combustor. Knowledge of the organic species produced during coal pyrolysis and the extent to which these species chemically react in the fluidized-bed combustor is required. It can be expected that both small aliphatic and polynuclear aromatic hydrocarbons could exist at temperatures of 850-950°C. Small hydrocarbons are formed directly by the cleavage of substituted alkyl groups, while polynuclear aromatic hydrocarbons are formed by the cleavage of bonds in the coal structural network. Branched and cyclic hydrocarbons are seldom products of coal pyrolysis above 800°C, and organic nitrogen and sulfur compounds decompose above 540°C to HCN or H_2S and small hydrocarbons. Although the diluted effluents (diluted 1000X) from the Exxon Miniplant stack were found to be nontoxic,[22] the particles suspended in the gas stream were in a respirable range and therefore have to be carefully screened for any specific polynuclear organic material which might be carcinogenic.

Trace elements emitted from fossil-fueled power plants have only recently received attention as potentially dangerous air pollutants. Although most trace elements present in the feed coal or limestone sorbent remain combined with the fly ash, the more volatile elements may be emitted with the stack off-gas as vapors or as adsorbed condensate on fly ash particulates that escape off-gas cleanup devices. The inorganic elements of special concern due to their toxic or carcinogenic nature are: Ag, As, Be, Cd, Co, Cr, Hg, Mn, Ni, Pb, Se, Sb, and Te. Possible enrichment of Be, Cr, Hg, Pb, and Se on fine fly-ash particulates is especially important. An investigation at Argonne National Laboratory[1] indicated that fluidized-bed combustion of coal produces less atmospheric emission of these elements (due to lower combustion temperatures) than does combustion of pulverized coal.

Studies have been undertaken on the radioactivity associated with the combustion of coal: (1) to find the fate of radionuclides in the coal fuel cycle; (2) to evaluate the concentration of ^{238}U, ^{234}U, ^{210}Pb, ^{210}Po, and Th; and (3) to study the release of radioactive material. The results tended to show that only 80% of the ^{234}U, ^{238}U, and ^{210}Pb present in the feed coal remained with the bottom ash after combustion. Therefore, collecting fly ash with electrostatic precipitators can reduce radionuclide emission. The

possible migration of radionuclides (especially U, Po, and Pb) and the emanation of ^{222}Ra from a bottom ash waste disposal pond could impose a pollution problem. Neither thorium nor radon was found in the fly ash.

The proposed studies in the present program include the following:

1. Identification of organic and inorganic constituents in effluent streams--their origin, fate, and biological role.

2. Identification of current FBC operating conditions that affect pollution. The amounts and kinds of pollutants will depend strongly on the composition of the coal and limestone used, as well as on the presence of additives.

3. Identification of methods of removing the pollutants. In order to destroy polyaromatic hydrocarbons, further oxidation will be necessary. A catalytic (Ni) burnup zone might be placed above the bed so that effluent leaving the bed would pass through it. This should not only decrease the amount of undesirable organic compounds, but also burn carbon and other particles. The organic and inorganic vapors in the effluent stream might be removed by condensation in a condenser placed downstream from the final filters. The condensation step additionally would work as a trap for any particulate escaping from the gas cleanup system. An alternative method for removing vapors of organic and inorganic species might be adsorption on sorbents such as ceramic or resin traps.

TASK C. LIMESTONE UTILIZATION

1. Enhancement of Limestone Utilization by Hydration
(J. A. Shearer, C. B. Turner, T. J. Prettyman, and K. M. Myles)

a. Laboratory Studies

In an investigation of the effects of chemical additives on limestone sulfation in fluidized-bed coal combustion, increased reactivity was correlated with pore structure changes.[21] Many chemicals were investigated; the major emphasis was on alkali- and halide-containing salts. $Ca(OH)_2$ as an additive was found to have some positive effects on some limestones (ANL/CEN/FE-78-10). Na_2SiO_3 was also tried with the expectation that the sodium would have some effect. However, only the hydrated silicate had an effect, suggesting that the presence of water during calcination may be the important variable. Hydrated clays have been shown to have effects on limestone decomposition.[23] Some work has also shown positive effects of increased levels of water vapor in the reacting gas phase.[24] $Ca(OH)_2$ itself has been used successfully as a sorbent for sulfur dioxide, however, handling problems and the economics of production of the material make it unsuitable as a sorbent for fluidized-bed combustion.[25,26]

(1) Effect of Hydration and Calcination on Sorbent Porosity

When pore structure changes induced by the use of chemical additives were correlated with increased reactivity, it was found that the formation of $Ca(OH)_2$ *in situ* was beneficial to a limestone previously sulfated to its maximum extent in a simulated flue gas. Application of this technique to fluidized-bed coal combustion could greatly improve utilization of the CaO in a limestone and reduce the quantity of solid waste generated. As part of a laboratory study, samples from process development unit (PDU)-scale experiments were examined for pore distribution changes. Figure 24 shows three curves, one for the original spent bed material ANL-9501 (26% sulfated), one for this material (HYS-1) hydrated for use as a feed sorbent, and one for the third sample consisting of final bed material (55-60% sulfated) generated by sulfation of the hydrated material. Two things to notice are (1) the shift to larger average pore diameter, indicated by the locations of the rises in the curve, *i.e.*, for the original spent material and for the final bed after water treatment and (2) the increase in total pore volume, indicated by the cumulative volume of the final-bed curve being greater than that of the original spent bed material. The formation of $Ca(OH)_2$ having twice the molar volume of the oxide caused the particles of limestone to expand. Upon calcination and dehydration of this material, the rapid loss of water created a new pore distribution, as well as recrystallized CaO of smaller grain size than in the original spent bed material. This increase in pore size and pore volume, as well as surface area, resulted in a material reactive to SO_2/O_2 so that resulfation led to greater total CaO utilization for the stone.

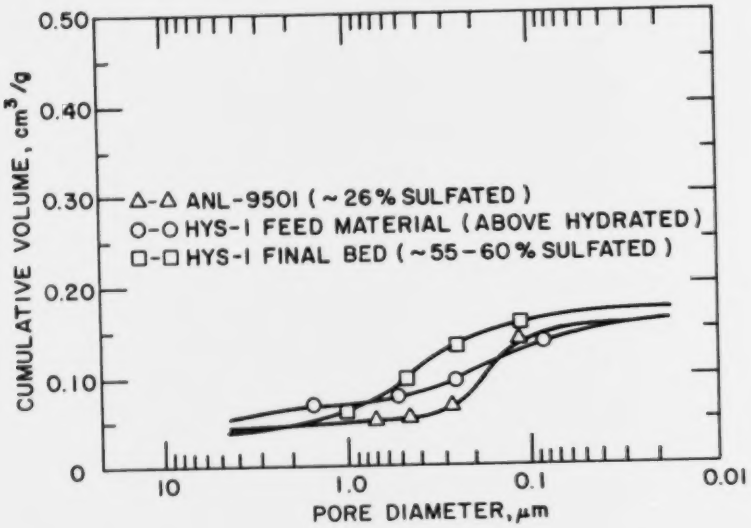

Fig. 24. Porosimetry Curves for ANL-9501 Showing the Effect of Water Treatment and Subsequent Resulfation on Partially Sulfated Fluidized-Bed Combustor ANL-9501 Samples

(2) Temperature and Method of Hydration

A scenario for using this technique for a large-scale plant would be cycling of overflow material into a fluidized-bed cooler-hydrator where pickup of water at temperatures lower than combustor temperatures would be expected to increase sorbent utilization upon recycle of the material into the combustor. Of economic concern is the temperature at which successful hydration can occur. The higher the hydration temperature, the more economical it will be due to less heat loss from cooling. Figure 25 shows the hydration of spent bed material from PDU-scale runs in a quartz fluidized-bed reactor, using water sprayed onto the bed surface, and its effect on porosity. The shifts to greater total volume and larger pore diameters resulted in sulfation increasing from 26% to 56% for spent limestone hydrated at 300-400°C. Hydrating at this high temperature would result in considerable savings over cooling the material to a much lower temperature.

For large amounts of material, steam injection rather than simple spraying may also be used as a method of hydration. Laboratory work has begun, using the quartz fluidized bed, with a water vapor feed attached to the lines containing fluidizing air flowing at about 3 scfm. Table 9 lists the percentages of water in samples of partially sulfated ANL-8001 (Greer limestone), experiment PER 700, from an atmospheric FBC and in two samples of ANL-9501 (Grove limestone) each of which had been sulfated in a different combustor--one in a pressurized system (experiment PFBC 9501) and one in an atmospheric FBC (experiment HYS-4). With a water feed of 110 g/h or more at 100°C, hydration of these materials can be achieved in several hours. The two ANL-9501 samples have markedly different initial sulfate

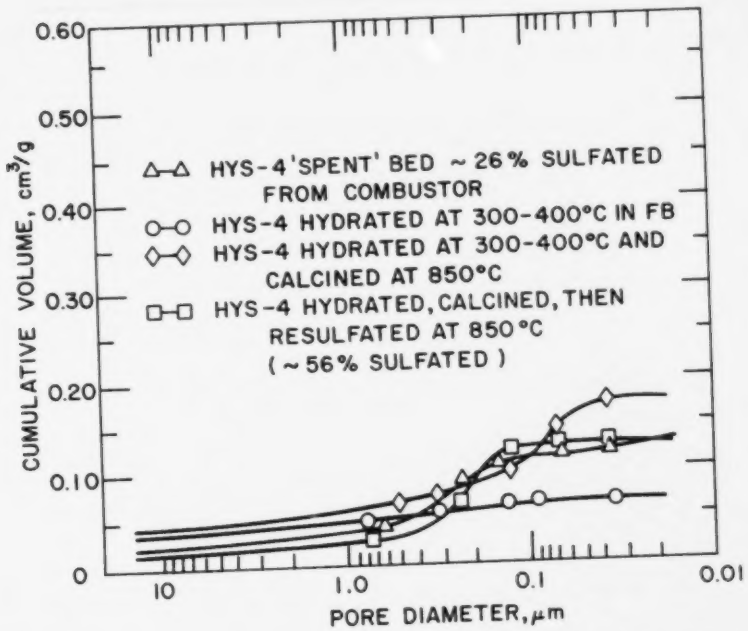

Fig. 25. Porosimetry Curves for Spent ANL-9501 Limestone (at 300°C) Sprayed with Water and Resulfated at 850°C in a Laboratory-Scale Fluidized Bed

contents. This difference is reflected in the amounts of hydration that occurred. The sample with the lowest sulfate content (HYS-4 with 26% sulfate) hydrated to a greater extent. Subsequent laboratory sulfations of all samples show significant increases in total sulfation after hydration--the exact values await analytical results. In some cases, water content decreased between the 2nd and 3rd hours. This is attributed to an inherent problem in sampling caused by fine material being selectively elutriated from the process vessel as hydration proceeded. There is some breakup of material, differing for different stones and the extent of hydration. After 3 h, the fine material, analyzed separately, had a higher water content than the coarse material remaining. The sample of coarse overflow showed a decrease in water content whereas the overall bed average showed an increase. Recorded here (Table 9) are water contents of overflow samples from the fluidized-bed.

These laboratory experiments in hydration of partially sulfated bed material are being extended to higher temperatures and to other materials. In a coal combustor system, the material to be treated will initially be at a higher temperature, and hydration at the highest possible temperature will be the most economical approach. A hydration temperature below 500°C but as close to this value as possible is most desirable. The earlier-mentioned spray technique was successful at higher hydration temperatures, and it is hoped that success at higher temperatures will apply to steam hydration as well.

Table 9. Laboratory Quartz Fluidized-Bed Hydration at 100°C of Partially Sulfated Limestone

Experiment (Stone Designation)	Rate of Water Addition, g H_2O/h	Duration of Hydration, h	Final Extent of Hydration in Stone, % H_2O
PER 700 (ANL-8001) ∿10-20% Sulfated	40	1	1.0
		2	1.5
		3	2.1
	110	1	1.4
		2	4.2
		3	4.8
	200	1	4.9
		2	5.6
		3	4.9
		3[a]	10.7
PFBC-9501 (ANL-9501) ∿56% Sulfated	110	1	0.8
		2	1.9
		3	2.1
HYS-4 (ANL-9501) ∿26% Sulfated	110	1	4.8
		2	6.2
		3	7.5

[a]Hydration of fines for 3h.

(3) Sulfation of Hydrated Sorbent

The technique of using in situ formation of $Ca(OH)_2$ in a partially sulfated "spent" limestone to further increase the extent of sulfation has been applied to a series of limestones and dolomites in laboratory-scale experiments. One-gram samples of stone were first precalcined and then exposed for 6 h to a simulated flue gas containing 0.3% SO_2 at 850°C. The reaction was essentially complete in this time; the partially sulfated material was then exposed to a water mist at room temperature, gaining 4-15% of weight (depending on the stone type) due to $Ca(OH)_2$ formation. The samples were then exposed for a further 6 h to the aforementioned simulated flue gas, and the resultant total extent of conversion of CaO to $CaSO_4$ was recorded. In most cases, the extent of sulfation after the second reaction due to the porosity contribution from dehydration was so great as to prohibit a second water treatment.

The numerical results are listed in Table 10, along with all data for the various dolomites and limestones tested and a visual evaluation of each stone's tendency to soften and powder when treated with water. The

Table 10. Enhancement of Sulfur Retention of Various Limestones and Dolomites[a] by Hydration Treatment (Tube Furnace)

Stone Identification,[b] ANL-	Calcium Conversion to $CaSO_4$, %[c] Partially Sulfated Sorbents	Resulfated Spent Sorbents[d]	Decrepitation
Limestone		Single Water Treatment	
7401	53.9	74.0	Minor
8001 (Greer)	34.0	70.9	Minor
8701	39.2	76.3	Medium
8901 (1343)	37.0	78.6	Major
9201 (1336)	20.7	68.6	Minor to Major
9501 (Grove)	13.6	74.6	Minor
9501 (AFBC Sample)	26.0	63.7	Minor
9603	12.8	71.4	Medium to Major
9701 (Germany Valley)	17.6	65.1	Minor
Dolomite			
5301 (Pfizer)	95.7	100.0	Minor
5401	41.6	70.3	Minor
5501	30.5	56.7	Minor
5601 (Dolowhite)	20.6	54.6	Minor
6101	68.5	100.0	Minor
6401	41.8	77.0	Minor
Cyclic Hydrations		Multiple Successive Water Treatments	
5501	30.5	50.8, 69.1, 82.0, 94.9, 100	
5601	20.6	51.3, 62.8, 73.9, 86.4, 96.9	
9501	13.6	79.7, 92.5, 97.7	

[a] One g sample, 18-20 mesh particle size, were sulfated in a simulated flue gas containing 0.3% SO_2 for 6 h at 850°C.

[b] The first two digits refer to the nominal wt % of $CaCO_3$ in the as-received stone.

[c] % = (analyzed moles S/analyzed moles Ca) × 100.

[d] Before resulfation, between 4 to 15 wt % water was added by mist spraying. Resulfation was for 6 h at 850°C in 0.3% SO_2, 5% O_2, 20% CO_2, and balance N_2.

first two digits of a stone's identification number refer to the percent $CaCO_3$ in the raw untreated material. The list included examples of both reactive and unreactive limestones and dolomites.

Two samples of dolomitic stones and a sample of one limestone whose potential for further sulfation was sufficiently great were exposed to water in successive treatments. ANL-5501 and ANL-5601 stones each reached about 100 percent conversion to sulfate after the second treatment of precalcined treated material. These two stones were used to compare precalcination followed by sulfation with simultaneous calcination/sulfation of the water-treated material. With precalcination a separate step, there is a much greater extent of sulfation in a short time than with simultaneous calcination/sulfation of a hydrated sample. ANL-9501 stone precalcined in a separate step quickly reached 100% conversion in three cycles.

Mercury porosimeter measurements were made on all samples for which pore size distribution of the final product differed greatly from that of the partially sulfated untreated starting material. After sulfation, the water-treated material has a broad distribution and a larger average pore size rather than a narrow pore size distribution. Changes in dolomite porosity as a result of water treatment are much smaller than for limestones.

On the basis of these investigations, the following conclusions may be made concerning laboratory-scale hydration of "spent" limestones and dolomites:

- Total porosity increases upon dehydration (molar volume of $Ca(OH)_2$ is approximately twice that of CaO)
- Average pore diameter increases (as a result of explosive removal of H_2O)
- Grain size decreases [upon recrystallization of CaO from $Ca(OH)_2$]
- Particle size increases (expansion) and/or decreases (decrepitation)
- Decrepitation increases (different for different stones)
- Sulfation increases (as a result of a more favorable pore distribution, a larger surface area)
- Surface area increases (total porosity increases, grain size decreases, pore size distribution changes)
- Dolomites undergo little or no decrepitation (water treatment has a very small effect physically due to the inert MgO present and the larger amounts of $CaSO_4$ initially present)

- Limestones, with some exceptions, generally have low to medium decrepitation (depends on percent $CaSO_4$, percent impurities including MgO, the method of water treatment, and the temperature of the stone when treated)

- Precalcination of the hydrated material as a separate step results in much more rapid and complete sulfation than does simultaneous calcination and sulfation.

(4) Characterization of Spent Sorbent, Calcined Sorbent, Hydrated Sorbent, and Recycled Sorbent

Work is continuing to characterize samples of water-treated limestones from the PDU-scale atmospheric combustor. The samples are from a series of cyclic experiments designed to maximize sulfation of limestone ANL-9501 by successive water treatments simulating continuous water treatment in a combustor system.

As part of the laboratory support for the process development unit at ANL, porosity distributions of material undergoing water treatment and sulfation in the combustor were measured. Figures 26-28 are the results from an experimental series of combustor runs in which a batch of ANL-9501 limestone was recycled after water treatment for a total of six sulfations at 850°C. Each sulfation run was kept at a steady state of 85% removal of sulfur

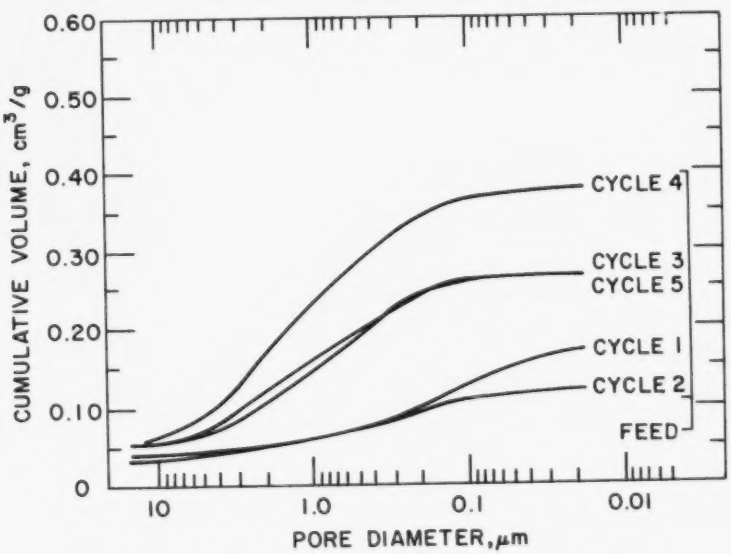

Fig. 26. Pore Distribution for Sulfated and Water-Treated ANL-9501 Sorbent Prior to Resulfation

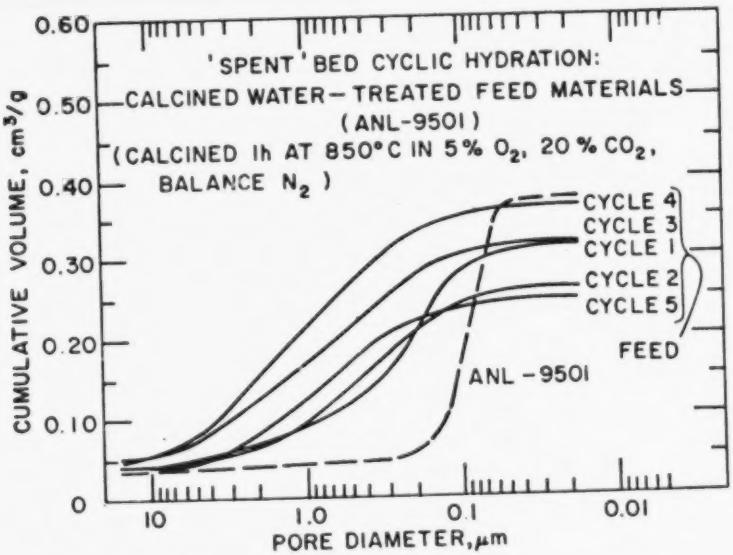

Fig. 27. Pore Distribution for Hydrated "Spent" ANL-9501 Sorbent after Calcination for 1 h at 850°C in 5% O_2, 20% CO_2, and the Balance N_2

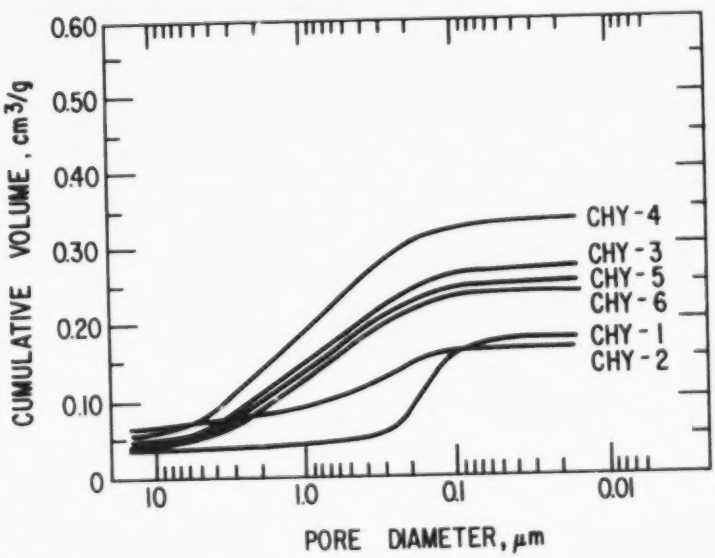

Fig. 28. Pore Distributions for Steady-State Overflow Samples of ANL-9501 Sorbent from Combustor at 850°C after Successive Cycles of Sulfation-Hydration

from the off-gas by suitable adjustment of the feed of recycled partially sulfated limestone. CHY-2 is sulfated stone that has been once-treated with water; CHY-3 is sulfated stone that has been twice-treated with water, etc.

Figures 26 and 27 show pore distributions for the feed material as fed (Fig. 26) and after 1 h calcination at 850°C (Fig. 27), illustrating the changes in pore structure upon firing. Also included in Fig. 27 is the porosity distribution of the original untreated calcined limestone, ANL-9501. After partial sulfation and water treatment, calcination results in dramatic changes in the porosity of CHY-2 and CHY-3 stone from the first two cycles. After the fourth cycle, CHY-4 material shows only a small increase in porosity in comparison to the uncalcined material reflecting the lower CaO content of the feed. CHY-5 and CHY-6 stones show even less change in porosity.

Figure 28 shows the porosity of steady-state samples taken from the combustor in each cycle, including CHY-1 (partially sulfated unhydrated material). As the number of cycles increased, the fraction of material sulfated increased and the CaO content decreased. In cycles CHY-5 and CHY-6, there was such a small contribution to porosity from the hydration of residual CaO that the porosity curve now reflected infilling of pore space due to the formation of $CaSO_4$. Hence, the curves for CHY-5 and CHY-6 show lower total porosity and, apparently, smaller average pore diameters.

Expansion of the particles and the increases in total porosity before sulfation, combined with an increasing surface area of pores larger than 0.3 μm, accounts for the increased sulfation during each cycle. Recrystallization of CaO to $Ca(OH)_2$ and back again serves to open up the pore structure and create greater surface area during each water treatment. Breaking-up of the surface and promotion of $CaSO_4$ crystal growth allows SO_2/O_2 mixtures to reach unreacted residual CaO. Thus, sulfation can proceed to virtual completion if there are enough cycles of hydration, calcination, etc.

In a combustor system having continuous recycling through a cooler/hydrator, overall sulfation would be better than sulfation without hydration, but would not reach 100% since continual withdrawal and feeding of bed material would result in an average sulfation value for the bed particles, some of which would be fully sulfated and others barely reacted.

In conjunction with the porosimetry studies, DTA measurements were performed on these samples with the intent of determining the distribution of the water between $CaSO_4$ hydrates and $Ca(OH)_2$. Figures 29 and 30 show low-temperature and high-temperature scans, respectively, of the cycled combustor materials. Results showed that almost 100% of the water is in the form of $Ca(OH)_2$ rather than hydrated calcium sulfate. In the low-temperature scans, only in CHY-5 material, which contained 85% $CaSO_4$, was there any noticeable contribution from the hydrated forms of $CaSO_4$. In fact, the positions of the CHY-5 peaks suggest that only adsorbed water comes off at these temperatures. Figure 30 shows that in each successive cycle, there is less $Ca(OH)_2$ present (which decomposes near 500°C), as would be expected because of the decreasing amount of CaO available and thus the smaller amount of water readily absorbed by the material.

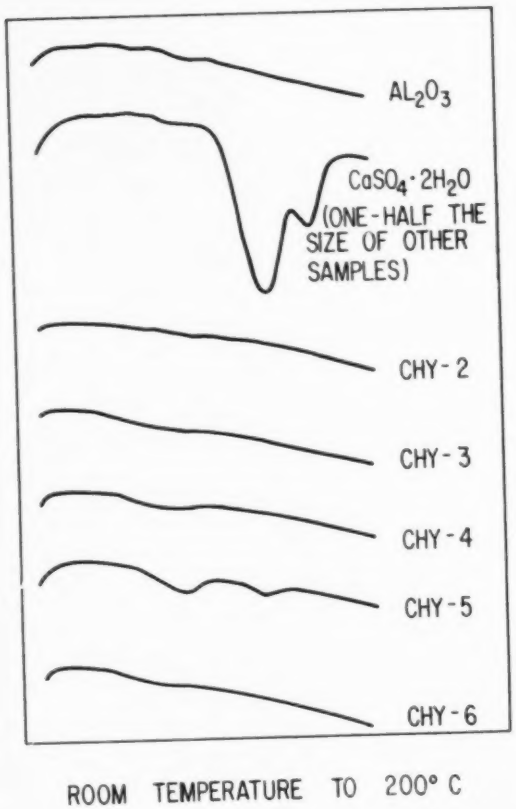

Fig. 29.

Low-Temperature DTA Curves for FBC Overflow Material. Feed, hydrated "spent" ANL-9501 limestone

Scanning electron microscopy is being used to characterize the materials. Figure 31 shows laboratory samples of hydrated "spent" limestone under conditions of (1) slow (gentle) hydration and (2) rapid hydration with vigorous production of steam from the heat generated by reaction. In both cases, the pore structure of the material changed dramatically as did the crystallite size of the material after dehydration and resulfation. Figure 32 shows two views of hydrated "spent" material after a second sulfation--again, large pores developed and there are small crystallites in the matrix. The rapid release of water of hydration from the $Ca(OH)_2$ created new pore structures and resulted in (1) rapid recrystallization of the CaO formed and (2) recrystallization and cracking of the $CaSO_4$ already present as a shell on the particle. Results of SEM studies on materials treated to cyclic hydration and sulfation will be presented in a future report.

2. Development of Process Flow Sheet for Spent Sorbent Hydration
(E. B. Smyk and W. M. Swift)

Although fluidized-bed combustion (FBC) offers a means of utilizing our vast coal resources in an environmentally acceptable manner to generate electric power and process steam, greater than stoichiometric quantities of sorbent are needed in this process, for SO_2 removal, with both economic and environmental impacts. Processes to increase sorbent utilization are being developed.

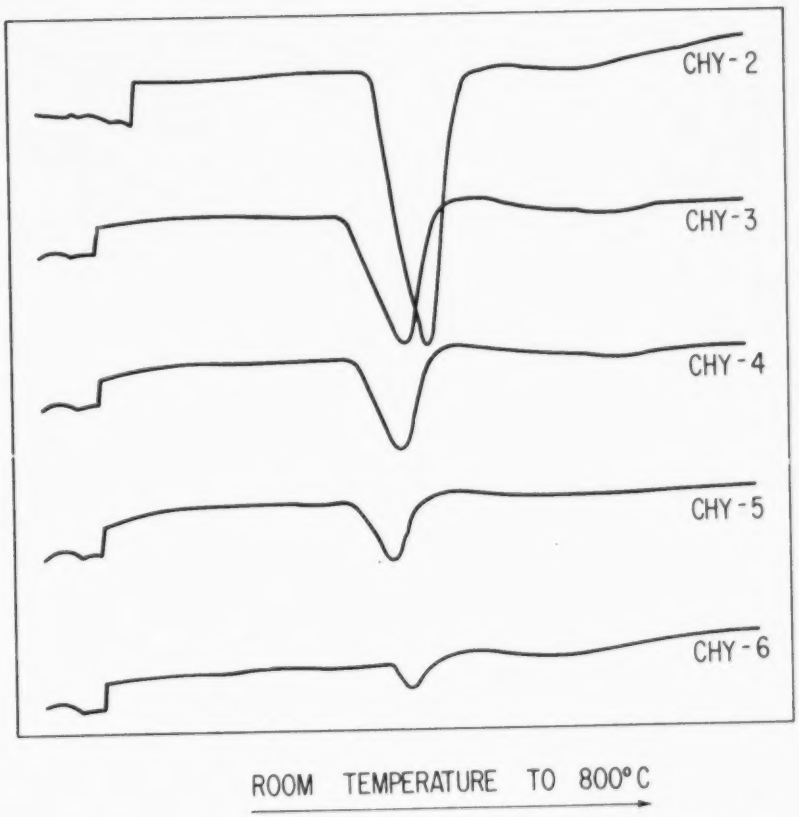

Fig. 30. High-Temperature DTA Curves for FBC Overflow Material. Feed, hydrated "spent" ANL-9501 limestone

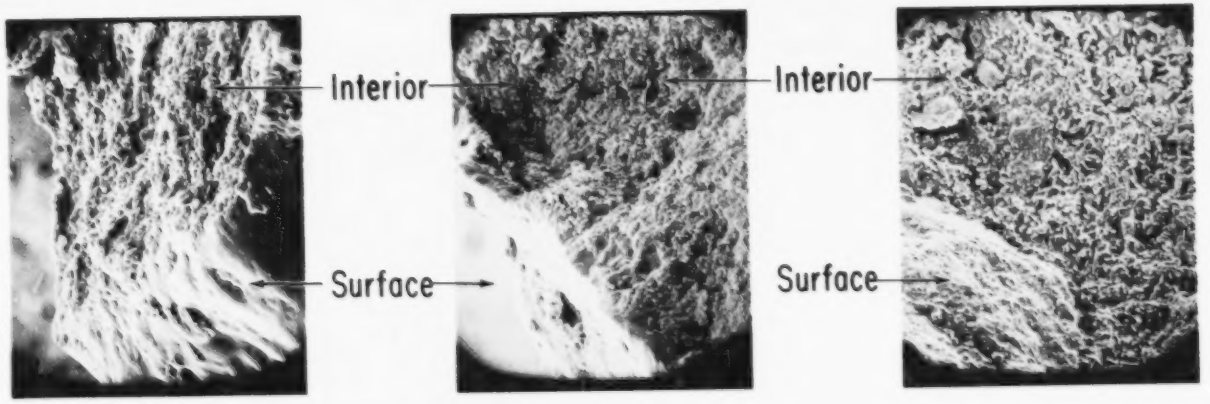

(a) Partially sulfated 9501 limestone 473X

(b) Gently hydrated 9501 (previously sulfated) 473X

(c) Vigorously hydrated 9501 (previously sulfated) 473X

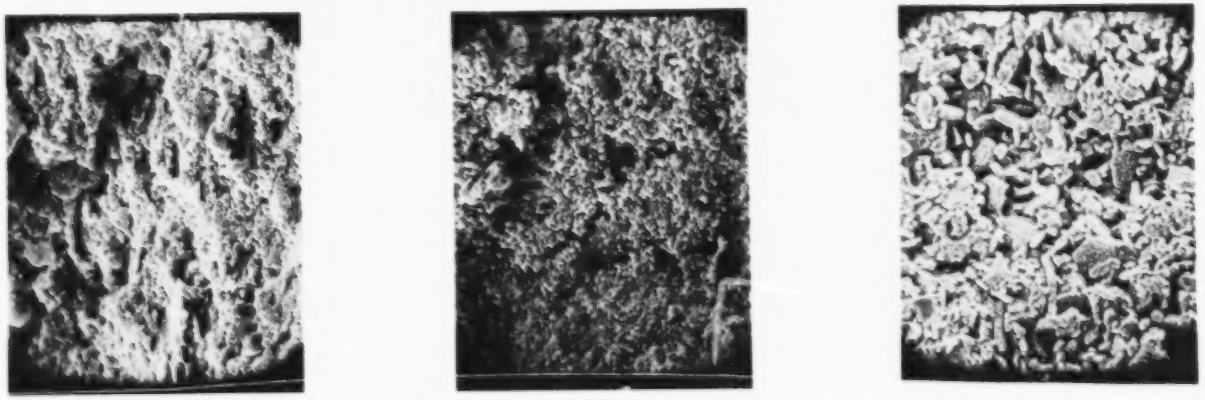

(d) Partially sulfated 9501 limestone interior view 946X

(e) Gently hydrated 9501 (previously sulfated) interior view 946X

(f) Vigorously hydrated 9501 (previously sulfated) interior view 946X

Fig. 31. Limestone ANL-9501 Partially Sulfated and Hydrated in a Laboratory Fluidized Bed

HYS-1 Final Bed
2200 X

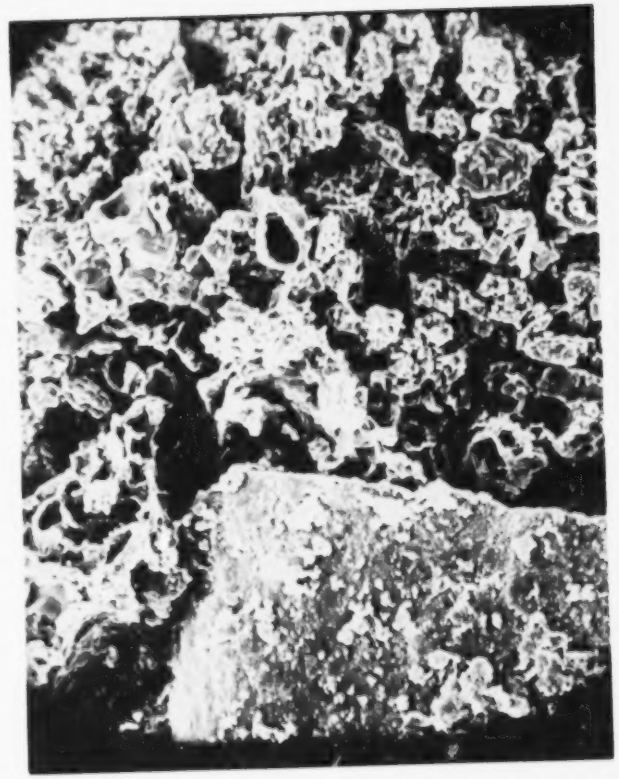

HYS-1 Final Bed
1100 X

Fig. 32. Two Views of a Particle of Limestone ANL-9501 (1359) After Being Partially Sulfated, Treated with Water, and Fed to a Fluidized-Bed Coal Combustor at 850°C. Note the expanded porosity.

In the process envisioned, partially sulfated sorbent from FBC is hydrated with water to increase its reactivity with SO_2. Laboratory-scale and PDU-scale tests have demonstrated that the reactivity of partially sulfated sorbent (heretofore unreactive) can be restored to nearly the same level as virgin sorbent by hydration (see preceding section).

It had been thought that hydration followed by dehydration of a lime sorbent within the FBC would yield a more open pore structure and that the sorbent would then be more reactive towards SO_2. However, material so treated was structurally weak and would crumble and elutriate when used in a fluidized bed. When this treatment was carried out on a partially sulfated lime sorbent rather than virgin lime, however, the calcium sulfate "shell" seemed to provide structural strength, allowing the particle to be hydrated and dehydrated without physical deterioration.

Previously, hydration had been carried out by spreading partially sulfated sorbent in shallow pans and spraying with water. This method would probably not be feasible in a large-scale system. Since the dehydration reaction (which occurs in the combustor) is endothermic, there would be less heat available in the combustor to generate steam. Thus, a process for hydrating the partially sulfated sorbent should also be capable of recovering the exothermic heat of hydration so that, ideally, there would be no net energy loss from the hydration-dehydration reactions.

When partially sulfated sorbent leaves the combustor, its temperature is about 1150 K. A significant amount of heat must be removed from this sorbent in order for it to be discarded at ambient temperature. It would be advantageous to develop a process for recovering this heat.

As shown in Fig. 33, the fluidized-bed cooler-hydrator (FBCH) performs both functions. Combustion air is sent through a fluidized bed of partially

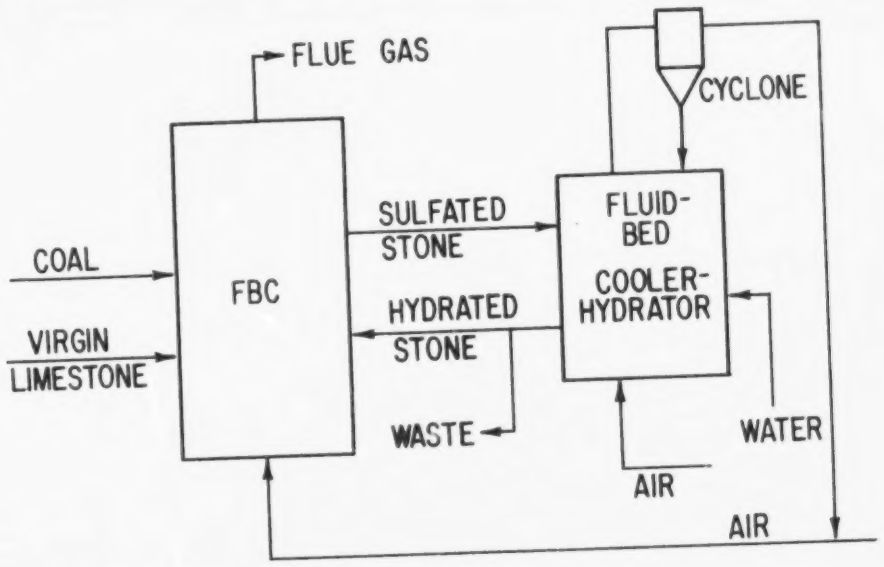

Fig. 33. Cooler-Hydrator for Water Treatment of Sulfated Sorbent

sulfated sorbent in the FBCH, along with water. Thus, both the sensible heat contained in the sorbent and the heat of hydration are transferred to the combustion air to preheat it and thereby increase the overall efficiency of the combustion cycle. Although $Ca(OH)_2$ has a decomposition temperature of 855 K and hydration should occur at any temperature below this, in practice, a considerably lower temperature may have to be employed to ensure hydration at appreciable rates without excessive amounts of water having to be used. Experimental work will be done to determine the optimum operating temperature for the FBCH.

Also, cyclic combustion-hydration experiments will be done to determine the effect of repeated combustion-hydration cycles on reactivity, attrition, and degree of hydration of the sorbent. Virgin sorbent will be sulfated in the combustor and then hydrated in the FBCH. The material taken from the FBCH will again be sent to the combustor and sulfated, after which it will be hydrated again. Recycling will be carried out in a batch mode (i.e., all material from Cycle 1 hydration will be saved and used as feed for Cycle 2 combustion, etc.) for about five or six cycles. From the results of these experiments, reactivity, attrition, and degree of hydration will be calculated as a function of cycle number, making it possible to design a continuous process and to determine the relevant fresh sorbent feed rate, circulation rate between combustor and cooler-hydrator, and waste production rate. These numbers should also make it possible to calculate rough cost figures for an economic evaluation of the hydration process.

3. Limestone Attrition Characterization
(W. I. Wilson and K. M. Myles)

Natural sorbents are being tested in a laboratory-scale fluidized-bed for their attrition resistance as a function of their physical and chemical properties (for example, the extent of calcination or sulfation, and the predominant grain size). The objectives of this study are (1) to determine the mechanism of attrition in fluidized beds and (2) to develop a relatively simple method of determining the attrition resistance of sorbents in fluidized-bed coal combustors.

The chemical analyses of the stones tested are given in Table 11, and the conversions of CaO to $CaSO_4$ are given in Table 12. Also included in Table 12 are the effect of calcination on the stone particle size, the estimated attrition resistance, and the predominant grain size.

a. Effect of Calcination

The effect of calcination on particle size was determined by selecting a batch of material, 1000-841 μm (-18 +20 mesh), and calcining it in a 20% CO_2-N_2 atmosphere at 900°C for approximately 30 to 45 min. The material was then sieved, and the actual size distribution (in wt %) was determined. The stones in these tests, in contrast to other stones previously tested under similar conditions, did not break up when calcined, i.e., the stones were not "poppers."

Table 11. Chemical Composition (wt %) of Limestone

Limestone Designation	$CaCO_3$	$MgCO_3$	Fe_2O_3	Al_2O_3	SiO_2	Na_2O	K_2O
ANL-5101	51.8	43.3	0.41	1.46	3.61	0.07	--
ANL-5301	53.4	45.4	0.07	0.08	0.69	0.05	--
ANL-6401	64.2	29.5	0.33	0.69	5.10	0.15	0.31
Meckley Limestone	66.3	4.0	3.91	2.31	15.86	--	--
ANL-8001	80.4	3.5	1.24	3.18	10.34	0.23	--
Lowellville Limestone	92.7	1.5	--	1.83	3.00	--	--
ANL-9501	95.3	1.3	0.09	0.25	0.77	0.03	--

The qualitative estimates of the probable resistance of each stone to attrition under fluidized-bed conditions were based on tests using a Pfizer tablet hardness tester. The results of the laboratory tests showed that the stones are similar in attrition resistance. However, from experimental observation and tests, calcination seemed to soften some stones, which may cause them to lose their integrity in fluidization tests. This softening was observed in ANL-5301 and the Meckley limestone. For example, after calcination, 89% of the starting ANL-5301 remained as 1000-841 μm particles in contrast to 95% of the ANL-8001, although in an actual fluidization test (2-h attrition in a cold fluidized-bed test of precalcined material), attrition of ANL-5301 and ANL-8001 caused a 34% loss and a 3% loss, respectively (the percent loss was determined as grams of overhead material × 100/gram of original material).

Following vacuum impregnation of each limestone sample with epoxy resin, polished sections were made of particles. These sections were examined in reflected polarized light. The results were compared with other stones prepared and examined under similar conditions. Average grain sizes were estimated (the estimates may be in error by a factor of two). To obtain an estimate, the predominant particle size of the grains in a sample was determined with a microscope and was assigned to one of three size categories (see footnote c of Table 12).

b. Test During Attrition Experiments

In a series of experiments, Tymochtee dolomite (ANL-5101) was tested to determine the effects of attrition on the distribution of particle size. Experiments were performed in a high-temperature (900°C) laboratory-scale

Table 12. Effect of Calcination, Sulfation, and Estimated Attrition Resistance in Fluidized Beds on Limestone Particles

Limestone Designation[a]	Size Distribution (wt %) after Calcination			Conversion of CaO to $CaSO_4$, %, in TGA[b]	Estimated Attrition Resistance[c]	Predominant Grain Size[d]
	1000–841 μm	841–595 μm	<595 μm			
ANL-5101	92.0	8.0	0.08	97.1	Medium	Medium
ANL-5301	89.0	10.0	1.4	96.8	Low	Medium
ANL-6401	92.3	6.1	2.7	62.6	Medium	Fine/Medium
Meckley Limestone	88.6	7.3	3.9	55.8	Low	Medium
ANL-8001	95.0	4.5	0.4	53.2	High	Fine
Lowellville Limestone	91.3	7.4	1.5	35.1	High	Fine
ANL-9501	91.0	8.0	0.4	37.5	High	Fine

[a] Initial particle size of limestone during each calcination test: 1000–841 μm.

[b] This column lists the percentages of calcium in the limestones (297–210 μm) converted to $CaSO_4$ after the stone has been precalcined in 20% CO_2 at 900°C and then reacted at 900°C with a 0.3% SO_2–5% O_2–20% CO_2–balance N_2 gas mixture for 5 h.

[c] Estimated by using a Pfizer tablet hardness tester.

[d] Fine: 4 to 63 μm across, Medium: 63 to 250 μm across.

fluidized-bed (quartz vessel) combustor. The experimental apparatus is schematically depicted in Fig. 34. The column has a 120 cm (48 in.) height in two sections. The bottom section is 45.7 cm (18 in.) high and has a diameter of 5.08 cm (2 in.). The top section is 76.2 cm (30 in.) high and has a diameter of 7.62 cm (3 in.). The top portion of the bed is a disengagement section that functions to decrease the velocity of the fluidizing gas and particles, minimizing particle entrainment. At the bottom of the bed, there is a porous metal plate that functions as a gas distributor. A pressure regulator controls the fluidizing gas flow. The experimental system also consists of a rotameter for monitoring the SO_2 concentration in the fluidizing gas, an external electric furnace for heating the bed, and a preheater for preheating some of the fluidizing gas. A cyclone and a filter located downstream from the bed collect the overhead particles.

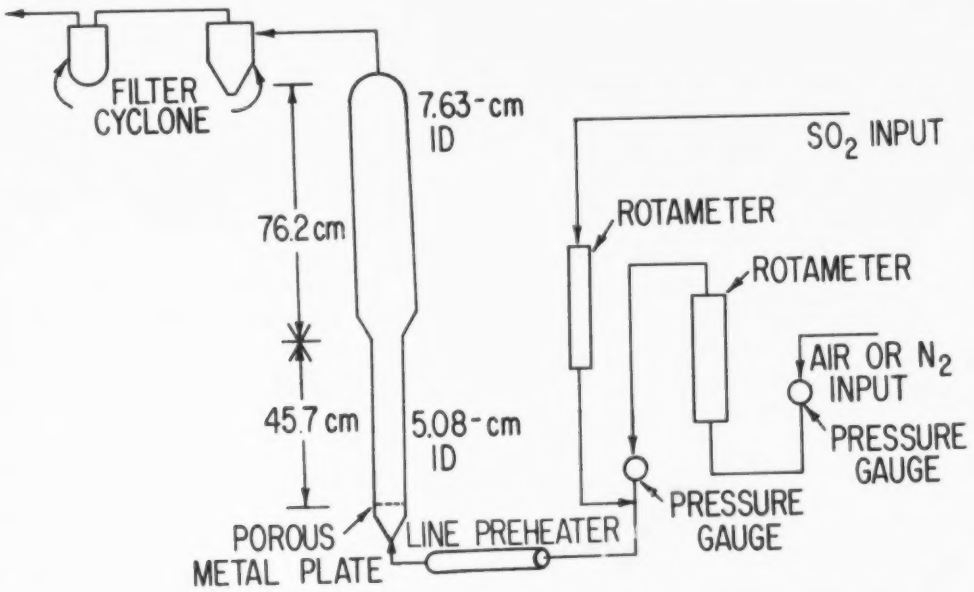

Fig. 34. Laboratory-Scale Fluidized-Bed Apparatus for Attrition Experiments

The sorbent was loaded into the combustion apparatus after sections of the bed were separated. The attrition tests were performed at approximately 875-900°C, using a fluidizing gas consisting of 0.3% SO_2-5% O_2 and the balance N_2.

Fluidized-bed attrition tests were run on two particle size ranges of Tymochtee dolomite, 1410-1190 μm (-14 +16 mesh) and 1000-841 μm (-18 +20 mesh). Cold virgin sorbent was charged to an empty hot bed (about 900°C) and then was fluidized for 15, 30, or 120 min, using a L/D of 1.25 (L/D of 1.38

in an expanded bed) and a superficial gas velocity of about 1.2 m/s. Subsequent sieve analyses gave a measure of the sorbent particle size distribution. The results are shown in Table 13 and in Figs. 35 and 36.

Table 13. Effect on Limestone Particle Size of Attrition in a Fluidized Bed at 900°C. L/D, 1.25; Superficial Gas Velocity, about 1.2 m/s

Initial Particle Size Before Attrition Test	Time of Run, min	Size Distribution After Attrition Test, wt %		
		(-14 +16 mesh) 1410-1190 µm	(-16 +30 mesh) 1190-595 µm	(-30 mesh) <595 µm
(-14 +16 mesh) 1410-1190, µm	15	64.2	35.4	0.4
	30	63.0	35.8	0.2
	120	53.6	46.1	0.3
		(-18 +20 mesh) 1000-841 µm	(-20 +30 mesh) 841-595 µm	(-30 mesh) <595, µm
(-18 +20 mesh) 1000-841 µm	15	85.5	14.3	0.2
	30	87.1	12.7	0.2
	120	83.0	16.8	0.2

Table 13 shows the size distribution after attrition tests for particle size ranges 1410-1190 µm and 1000-841 µm. For the 1410-1190 µm diameter material, approximately 63 wt % of the particles for the 15 and 30 min tests retained their original diameters at the end of the attrition tests. There is a slight decrease in particle diameter in the 120 min test. For the particle size range, 1000-841 µm, 85 wt % of the particles had the same particle diameters as the original starting bed material at the end of the 15, 30, and 120 min attrition tests. When the results for the two particle size ranges are compared, it can be seen that there is a greater shift in the particle diameter for the 1410-1190 µm material than for 1000-841 µm material. The amounts of material smaller than 595 µm for all six runs (in both particle size ranges tested) were small (0.2 to 0.4%).

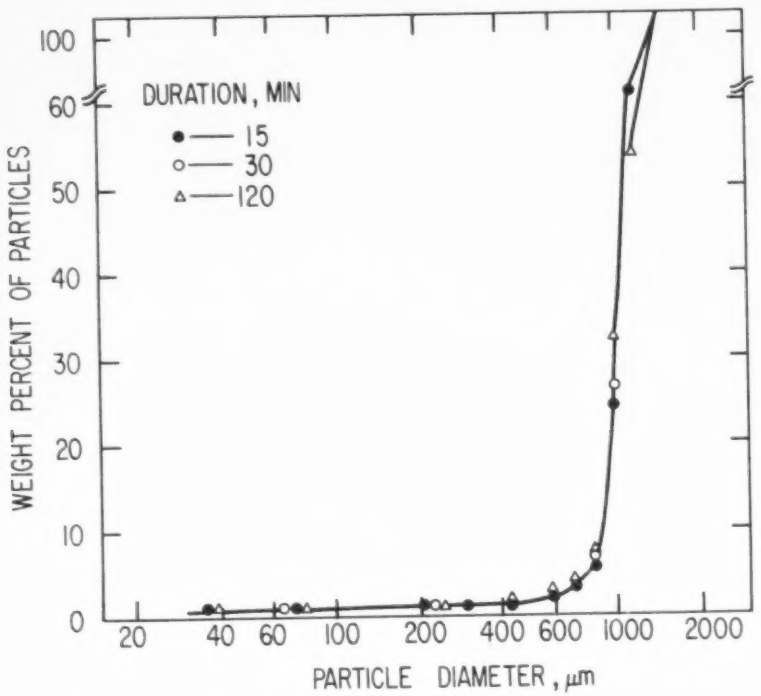

Fig. 35. Particle Size Distribution of ANL-5101 (Tymochtee dolomite). Simultaneous calcination and sulfation after attrition tests of given durations. Initial particle diameter, 1410-1190 μm

Figures 35 and 36 are graphs of the weight percent of particles vs. particle diameter. Figure 35 shows the curve for 1410-1190 μm material, and Fig. 36 shows the curve for 1000-841 μm material. In the tests at both size ranges, the plots suggest that after 15 min, the attrition rate was constant (at zero) during all test runs.

Further testing is planned in order to delineate the source of attrition as a function of particle size distribution. Tymochtee dolomite (ANL-5101) and other limestones will be used. These tests will be designed to test the sorbent at shorter residence times and with a lower SO_2 concentration in the fluidizing gas.

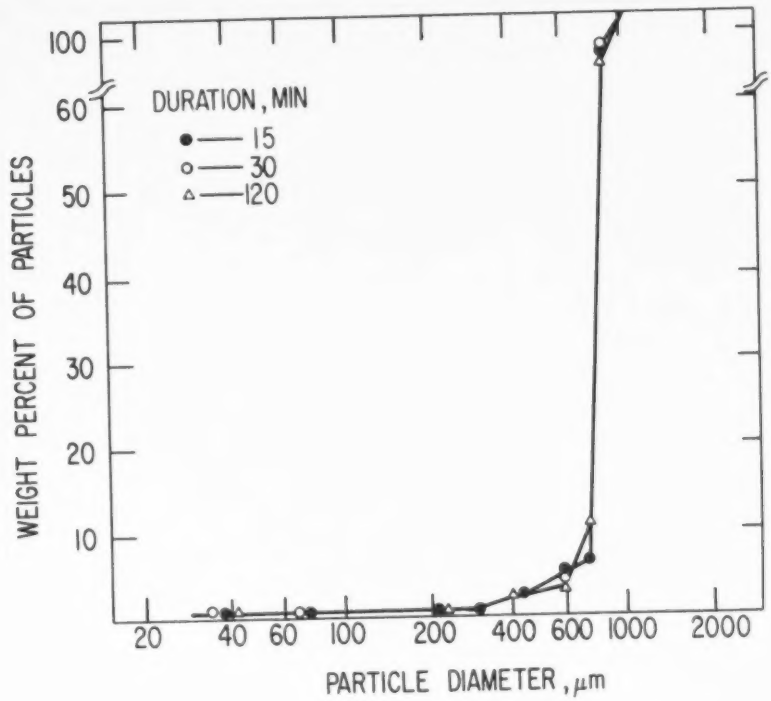

Fig. 36. Particle Size Distribution of ANL-5101 (Tymochtee dolomite). Simultaneous calcination and sulfation after attrition tests of given durations. Initial particle diameter, 1000-841 μm

4. Studies of Sulfation Process in FBC
(J. A. Shearer, C. B. Turner, and K. M. Myles)

Partially sulfated limestone samples from the 6-in.-dia atmospheric fluidized-bed coal combustor have been examined under a scanning electron microscope (SEM) for future comparison with laboratory samples generated without coal combustion.

Table 14 lists operating conditions (in the fluidized-bed combustor) common to all samples; differences in conditions were the manner of their treatment and the temperature of combustion.

Figure 37 shows three ANL-9501 limestone particles fired in the atmospheric fluidized-bed coal combustor at three different temperatures with no salt addition. The porosity developed upon calcination and sulfation can be seen to increase slightly at two higher temperatures. The extent of sulfation is similar at the higher temperatures, but lower at 800°C due to incomplete calcination. Figure 38 shows a cross section of a particle from the 800°C run; a large amount of uncalcined $CaCO_3$ is present that has recrystallized into discrete rhombic grains and has not yet lost its CO_2. The partial

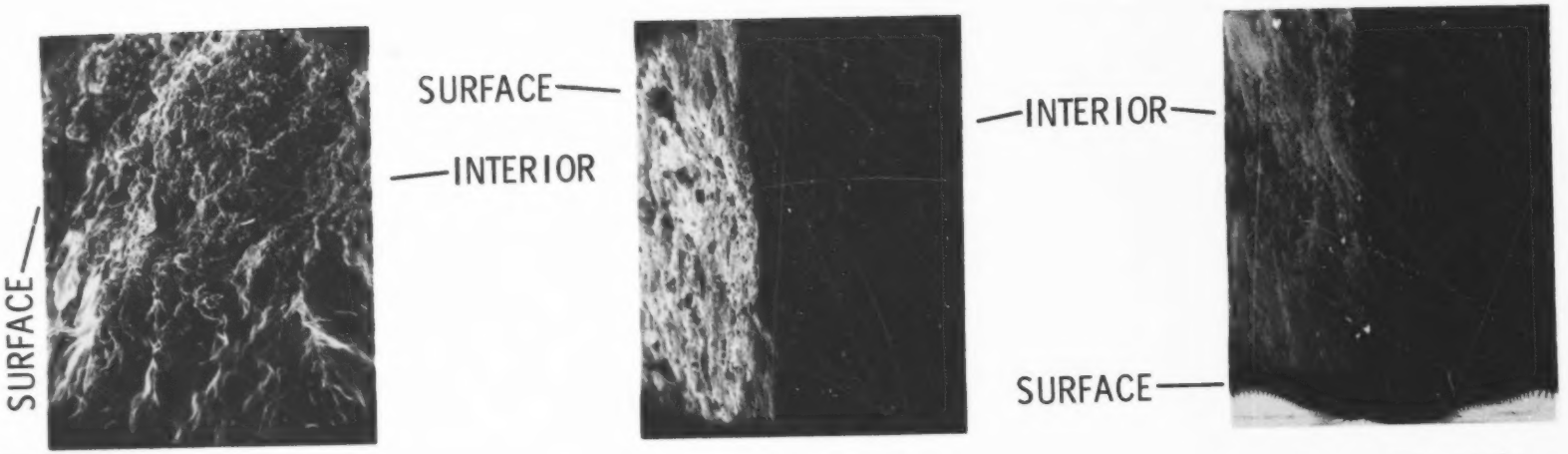

Expt. SG6A 800°C
627X

Expt. CT-1 850°C
627X

Expt. SG7A 900°C
627X

Fig. 37. Sulfated ANL-9501 (1359) Particles Produced at Different Bed Temperatures in the Atmospheric Fluidized-Bed Coal Combustor. ANL Neg. No. 308-79-71

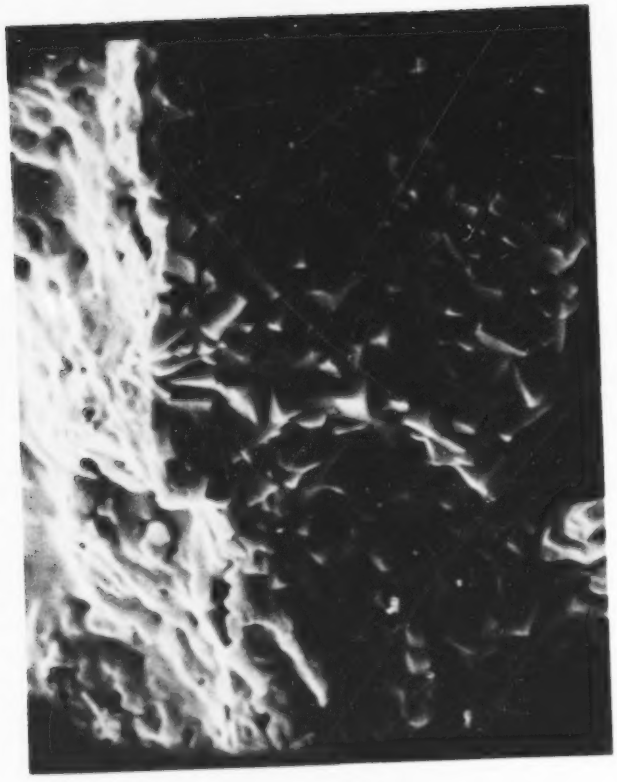

Expt. SG6A 800°C
5500X

Fig. 38. Interior View of ANL-9501 Particle, Sulfated in Fluidized-Bed Coal Combustor at 800°C, Showing Uncalcined Limestone. ANL Neg. No. 308-79-67

Table 14. Operating Conditions for 6-in.-dia Fluidized-Bed Coal Combustor with Various Sorbent Feeds

Pressure:	101.3 kPa (1 atm)
Fluidizing-gas velocity:	1 m/s
Fluidized-bed height:	813 mm
Excess Air:	3% O_2 in dry off-gas
Coal:	Sewickley (-12 +100 mesh) containing 5.5% S
Sorbent:	Grove limestone ANL-9501 (-10 +30 mesh) containing 93.3% $CaCO_3$

pressure of CO_2 at 800°C in the fluidized-bed coal combustor can be high enough to prevent complete calcination, thereby preventing the development of porosity and the sulfation of CaO.

Figure 39 shows porosimetry curves for these same samples. The pore distribution for the 900°C sample is shifted to larger average pore diameters in comparison to the sample fired at 850°C. The 800°C sample has a very low total porosity due to the incomplete calcination shown in Fig. 38. Characterization of combustor samples will continue in order to obtain a firm basis for clarifying differences in the reactivities of limestone sulfated in combustors and in simulated flue gas in laboratory apparatus.

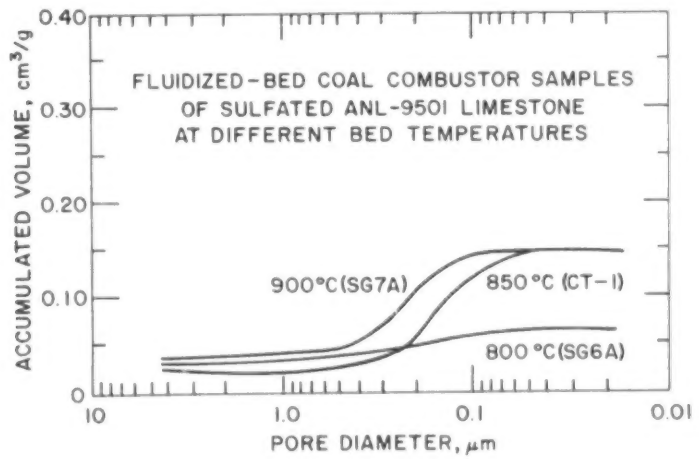

Fig. 39. Porosimetry Curves for Fluidized-Bed Coal Combustor Samples of ANL-9501 Limestone Sulfated at Different Bed Temperatures

REFERENCES

1. W. M. Swift, G. J. Vogel, A. F. Panek, and A. A. Jonke, Trace-Element Mass Balances Around a Bench-Scale Combustor, Proceedings of the 4th International Conference on Fluidized-Bed Combustion, The Mitre Corp., Virginia, May 1976, pp. 525-543.

2. National Coal Board, London, Britain, Reduction of Atmospheric Pollution Reducing Emission of Sulfur Oxides, Nitrogen Oxides and Particulates by using Fluidized Combustion of Coal, Report to U.S. EPA, Three volumes, PB 210-637, PB 210-674, PB 210-675 (September 1971).

3. K. E. Phillips, Energy Conversion from Coal Utilizing CPU-400 Technology, Annual Report for July 1975-June 1976, FE-1536-A-2, Combustion Power Company, Menlo Park, California.

4. An Investigation of Hot Corrosion and Erosion Occurring in Fluidized-Bed Combustor-Gas Turbine Cycle Using Coal as Fuel, Report to U.S. ERDA, FE/1536-2 (May 1977).

5. R. L. McCarron, A. M. Beltran, H. S. Spacil, and K. L. Luthra, Turbine Materials Corrosion in the Coal-Fired Combined Cycle, The Proceedings of the Fifth International Conference on Fluidized-Bed Combustion, Washington, D.C., December 12-14, 1977, Vol. III - Developmental Activities, pp. 714-736.

6. S. H. D. Lee and I. Johnson, Removal of Gaseous Alkali Metal Compounds from Hot Flue Gas by Particulate Sorbents, paper presented at 24th Annual International Gas Turbine Conference at San Diego, California, March 11-15, 1979, paper No. 79-GT-154.

7. S. Brunauer, The Adsorption of Gases and Vapors, Vol. 1, Physical Adsorption, Princeton University Press, p. 13 (1945).

8. J. G. Vail, Ed., Soluble Silicates--Their Properties and Uses, 1st ed., Reinhold Publishing Corporation, N.Y. (1952).

9. R. K. Iler and E. J. Tauch, Sodium Silicate and Hydrochloric Acid from Sand, Salt, and Steam, Trans. Am. Inst. Chem. Eng. 37, 853-877 (1941).

10. W. T. Reid, Ed., External Corrosion and Deposits--Boilers and Gas Turbines, 1st Ed., American Elsevier Publishing Comp., Inc., New York (1971).

11. W. Nelson and E. S. Lisle, High-Temperature External Corrosion on Coal-Fired Boilers: Siliceous Inhibitors, J. Inst. Fuel 38, 179-186 (1965).

12. W. M. Swift, S. H. D. Lee, J. C. Montagna, G. W. Smith, I. Johnson, G. J. Vogel, and A. A. Jonke, Plans and Studies on Flue Gas Cleaning and Particulate Monitoring in PFBC, presented at the 5th International Conference on Fluidized-Bed Combustion, Dec. 12-14, 1977, Washington, D.C., Part III.

13. Kirk-Othmer Encyclopedia of Chemical Technology, 2nd Ed., Vol. 18, Interscience Publishers, New York, p. 134 (1963).

14. S. K. Chirkov, The Preparation of Water Glass without the Use of Alkalies, J. Chem. Ind. (Moscow) 13, 469-474 (1939).

15. D. L. Keairns et al., Fluidized Bed Combustion Process Evaluation, EPA Report EPA-650/2-75-027-C (1975).

16. General Electric Company, Assessment of Gas Turbine Erosion, New York State Energy Research and Development Authority - General Electric Company Agreement dated March 31, 1977, Monthly Progress Report (April 1979) (to be published).

17. D. S. Scott, W. M. Swift, and G. J. Vogel, Pulse-Jet Acoustic Dust Conditioning in High-Temperature/Pressure Applications, Proc. EPA/ERDA Symp. on High-Temperature/Pressure Particulate Control, Washington, D.C. (September 1977).

18. D. S. Scott, J. Sound Vib. 43, 607 (1975).

19. R. Razgaitis, An Analysis of the High-Temperature Particulate Collection Problem, Argonne National Laboratory Report ANL-77-14 (1977).

20. C. K. Groves, The Development of a Pulse-Jet Driven Acoustical Dust Conditioner for High Temperature/Pressure Application, B.A. Sc. thesis, Division of Eng. Sci., Faculty of Appl. Sci. and Engr., Univ. of Toronto (March 1978).

21. J. A. Shearer, Irving Johnson, and C. B. Turner, The Effect of Sodium Chloride on the Reaction of SO_2/O_2 Mixtures with Limestones and Dolomites, Argonne National Laboratory ANL/CEN/FE-78-8, June 1978.

22. J. M. Allen and K. M. Duke, Multimedia Emissions from Pressurized FBC of Coal, 71st Annual Meeting Air Pollution Control Assn., Houston, June 1978.

23. K. P. Kacher, R. C. Satiya, and D. Chandra, Zem. Kalk. - Gips 25(1), 37-41 (1972).

24. R. T. Yang, A. S. Albanese, J. M. Chen, G. Farber, F. B. Kainz, J. Pruzansky, M. S. Shen, R. Smol, and M. Steinberg, Regeneration Process for Desulfurization of High Temperature Combustion and Fuel Gases, Quarterly Progress Report No. 6, Brookhaven National Laboratory, July 1-September 30, 1977, BNL-50750.

25. H. L. Falkenberry and A. V. Slack, Chem. Eng. Prog. 65(12), 61-66 (1969).

26. A. E. Potter, Am. Ceram. Soc. Bull. 48(9), 855-858 (1969).